



Solvent, structural, quantum chemical study and antioxidative activity of symmetrical 1-methyl-2,6-bis[2-(substituted phenyl)ethenyl]pyridinium iodides

Milena D. Milošević¹ · Nevena Ž. Prlainović² · Miloš Milčić³ · Vesna Nikolić³ · Aleksandra Božić⁴ · Miljan Bigović⁵ · Aleksandar D. Marinković¹

Received: 20 December 2017 / Accepted: 22 June 2018
© Iranian Chemical Society 2018

Abstract

15 symmetric 1-methyl-2,6-bis[2-(substituted phenyl)ethenyl]pyridinium iodides were synthesized in this work. Their structures were characterized using IR, ¹H and ¹³C NMR, and UV–Vis spectroscopy. DFT calculations indicated that *s-trans/s-trans* conformation prevail in all compounds. The effects of specific and non-specific solvent–solute interactions on the UV–Vis absorption maxima shifts were evaluated using linear solvation-free energy relationships (LSER), i.e., Kamlet–Taft and Catalán models. A linear free energy relationship (LFER) in the form of single substituent parameter equations (SSP) was used to postulate quantitative structure–property relations of substituent effect on NMR data. TD-DFT results showed dependence of electronic transition on the substituent effects. The push–pull character of these compounds was analyzed by differences in ¹³C chemical shift of the ethylenic double bond in 2- and 6-positions of cross-conjugated with pyridinium central ring. Also, the quotient of the occupations for the bonding π and anti-bonding π^* orbitals of this bond was considered. Good correlations of the selected parameter between double bond lengths with π^*/π and ¹³C chemical shift differences of the bridging group proved them to be adequate descriptor of push–pull character. Synthesized compounds were screened for the antioxidant activity, using 1,1-diphenyl-2-picrylhydrazyl (DPPH) and 2,2'-azino-bis(3-ethylbenzothiazoline-6-sulfonic acid) (ABTS) radical methods, and results demonstrated moderate antioxidant potential.

Keywords Solvatochromism · Kamlet–Taft · Catalán · Antioxidant activity

Electronic supplementary material The online version of this article (<https://doi.org/10.1007/s13738-018-1437-5>) contains supplementary material, which is available to authorized users.

✉ Milena D. Milošević
milenamiloševictmf@gmail.com
Aleksandra Božić
aleksandrabožictmf@gmail.com

- ¹ Faculty of Technology and Metallurgy, University of Belgrade, Karnegijeva 4, 11000 Belgrade, Serbia
- ² Innovation Centre of Faculty of Technology and Metallurgy, University of Belgrade, Karnegijeva 4, 11000 Belgrade, Serbia
- ³ Faculty of Chemistry, University of Belgrade, Studentski trg 12-16, 11000 Belgrade, Serbia
- ⁴ Belgrade Polytechnic, Brankova 17, 11000 Belgrade, Serbia
- ⁵ Faculty of Science and Mathematics, University of Montenegro, Bulevar Džordža Vašingtona bb, 81000 Podgorica, Montenegro

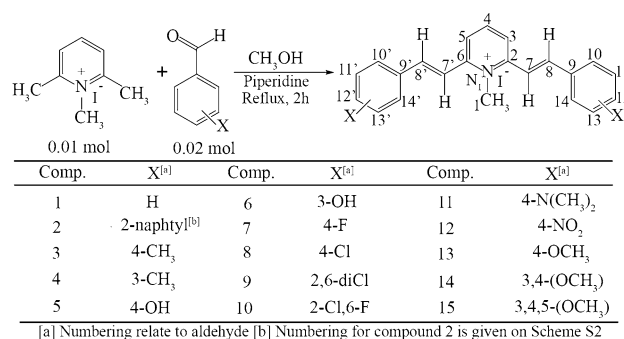
Introduction

Development of new technologies over the past several years resulted in craving for the synthesis of new compounds and materials with promising application in biology and medicine. Compounds able to interact directly with nucleic acids are of great importance in cancer chemotherapy. In particular, molecules able to exert their biological effects by binding reversibly to the receptors include aromatic or heteroaromatic moieties. In that context, systems which belong to the class of the so called push–pull (donor–acceptor system, D–A) molecules have attracted a great attention. The study of this class of compounds is growing tremendously with particular focus on the pyridine and its derivatives. Due to their aromatic structures, high dipolar interaction and strong electronegativity arising from the presence of nitrogen atom, derivatives of pyridine molecule show significant biological activity. Fortunately, simple syntheses of the

aromatic aldehydes with pyridines provide an opportunity for easy preparation and modification of the desired chemical structures [1]. Thus, chemical modification by various heteroaromatic substituents provides derivatives that possess the ability to contribute to lung A549 and breast X226 cancer therapy [2, 3]. Some derivatives have attracted significant interest after numerous in vitro and in vivo studies showed their antiproliferative [2, 4] and antioxidant activity [5–7]. In addition, due to their mentioned structure as push–pull molecules, researchers expanded their application in other fields of science and technology such as: nanotechnology, optics and optoelectronics, analytical, and environmental sciences [8, 9]. They are, also, used as non-linear optical materials, as fluorescent probes [1, 9–11].

Compounds containing styrene unit connected to a pyridine ring are an important class of organic molecules endowed with a highly polarizable π -electron system. Due to their interesting biological activity, spectroscopic, photo-physical and photochemical properties thousands of different styryl compounds have been investigated [1, 12–14]. To study specific properties of styryl derivatives, it is essential to fully characterize molecular structure and obtain valuable information from the spectroscopic results. Therefore, several spectroscopic techniques have been developed and applied to investigate structure peculiarity, i.e., the position of pyridine nitrogen, conjugation throughout the molecule, and rotational isomerism [15–17]. Spectral and photochemical studies in a variety of solvents confirmed dynamic equilibrium of different conformational isomers, and therefore they showed complex UV–Vis spectra. Even more complex behavior, compared to the most commonly studied neutral molecules, shows their pyridine salts. Methylation of the pyridine nitrogen atom converts those molecule to a cross-conjugated systems with better performances as non-linear optic materials [18].

In this study, the synthesis of the 15 symmetric 1-methyl-2,6-bis[2-(substituted phenyl)ethenyl]pyridinium iodides, i.e., 1-methyl-2,6-bis(substituted styryl)pyridinium iodides (Scheme 1), is presented. UV–Vis spectra, recorded in 20 solvents of various polarity, were used for studying solute/solvent interactions by the use of linear solvation energy relationships (LSER) using both Kamlet–Taft and Catalán models. The linear free energy relationship (LFER) principles were applied to get an insight into factors influencing NMR chemical shifts and ν_{\max} value. DFT/TD-DFT was used for geometry calculations and analysis of the extent of ICT during excitation. Calculations of the bond lengths and occupying coefficient were used for the quantification of the push–pull effect. According to this concept, appropriate conclusions of the substituent effects, steric hindrance, and push–pull character of the compound have been made. In addition, synthesized compounds were



Scheme 1 Reaction path of 1-methyl-2,6-bis[2-(substituted phenyl)ethenyl]pyridinium iodides synthesis

investigated for their antioxidant potential using DPPH and ABTS methods.

Experimental section

Materials and characterization methods

Details on materials and characterization methods are given in Supplementary materials.

Synthesis of symmetrical 1-methyl-2,6-bis[2-(substituted phenyl)ethenyl]-pyridinium iodide (1–15)

The series of symmetrical compound 1–15 was synthesized by the condensation reaction of *N*-methyl-2,6-lutidine iodide and appropriate aromatic aldehyde (Scheme 1). The description of the syntheses of 1-methyl-2,6-dimethylpyridinium iodide is given in the Supplementary Material (Scheme S1) [13]. Compounds 1 [19], 5 [13], and 11 [20] have, already, been known in the literature. All the compounds presented in this work were synthesized according to the modified literature procedure [13], and their purity was verified through a melting point determination and elemental analysis. We found that the solubility of product was better in methanol/piperidine mixture instead of ethanol/piperidine mixture, as described previously [13]. Therefore, with better solubility higher product yields (44–67%) were obtained in only 2 h instead of 3 days. A detailed description of the experimental procedures and the characterization of reported compounds are given in the Supplementary Material.

Detail characterization of known compounds is given in Supplementary Material, while data of newly synthesized compounds are reported below. 1-D (¹H and ¹³C, Figs. S1–S4) spectra of the selected compounds are also given in Supplementary Material. Atom numbering of synthesized compounds is outlined in Scheme 1.

1-Methyl-2,6-bis[2-(2-naphthyl)ethenyl]pyridinium iodide (2)

Yellow powder; yield: 67%; m.p. 253 °C, Elem. Anal: Calcd. for $C_{30}H_{24}IN$ ($M_w = 525.42$ g mol⁻¹): C, 68.58; H, 4.60; N, 2.67%. Found: C, 69.08; H, 5.10; N, 3.17%; IR (KBr, cm⁻¹): 3042 (C–H stretching of pyridine group), 2924 (=N⁺–CH₃ stretching), 2853 (C–H stretching of –CH₃ group attached to nitrogen), 1610, 1568, (C=C stretching of aromatic ring), 1488 (C=C asymmetric stretching of aromatic ring), 1248, 1173 (C–N stretching of pyridine ring), 966 (=CH assigned to out-of-plane deformation of *trans* alkenes), 775 (–CH out-of-plane deformation of phenyl group); ¹H-NMR (200 MHz, DMSO-*d*₆, δ/ppm): 4.31 (3H, *s*, =N⁺–CH₃); 6.91 (2H, *d*, *J* = 7.2 Hz, CH=CH), 7.38–7.45 (6H, *m*, CH=CH, pyridine and C₆H₄), 7.63 (4H, *dd*, *J* = 7.9 Hz, *J* = 5.6 Hz, C₆H₄), 7.80–7.85 (4H, *m*, C₆H₄), 8.00 (4H, *dd*, *J* = 6.8 Hz, *J* = 5.1 Hz, C₆H₄), 8.30–8.36 (4H, *m*, C₆H₄), 8.45 (1H, *br.m.ovl.*, pyridine); ¹³C-NMR (50 MHz, DMSO-*d*₆, δ/ppm): 41.5 (=N⁺–CH₃), 124.5 (C₇), 128.2 (C₃), (C₅) 128.6 (C₁₄), 129.2 (C₁₃), 130.0 (C₁₇), 130.4 (C₁₆), 133.2 (C₁₈), 113.9 (C₁₅), 134.2 (C_{12a}), 134.6 (C₈), 138.2 (C₉), 138.6 (C₁₁), 153.6 (C₄), 155.8 (C₂).

1-Methyl-2,6-bis[2-(4-methylphenyl)ethenyl]pyridinium iodide (3)

Yellow crystal; yield: 55%, m.p. 203.8–208.8 °C, Elem. Anal: Calcd. for $C_{24}H_{24}IN$ ($M_w = 453.36$ g mol⁻¹): C, 63.58; H, 5.34; N, 3.09%. Found: C, 64.08; H, 5.69; N, 3.59%; IR (KBr, cm⁻¹): 3050 (C–H), 2917 (=N⁺–CH₃), 2857 (C–H), 1615, 1560 (C=C), 1483 (C=C), 1449 (C–H), 1287, 1246 (C–N), 979 (=CH), 809 (C–H); ¹H-NMR (200 MHz, DMSO-*d*₆, δ/ppm): 2.37 (6H, *s*, –CH₃), 4.28 (3H, *s*, =N⁺–CH₃), 7.32 (2H, *s*, *J* = 8.0 Hz, CH=CH), 7.65 (2H, *d*, *J* = 8.0 Hz, CH=CH), 7.68–7.74 (6H, *m*, pyridine and C₆H₄), 8.26 (4H, *d*, *J* = 7.4 Hz, 2C₆H₄), 8.42 (1H, *dd*, *J* = 8.0 Hz, *J* = 5.6 Hz, pyridine); ¹³C-NMR (50 MHz, DMSO-*d*₆, δ/ppm): 22.4 (–CH₃), 40.5(=N⁺–CH₃), 124.3 (C₇ and C₇), 128.3 (C₃ and C₅), 128.9 (C₁₀, C₁₄, C₁₀, and C₁₄), 129.1 (C₁₁, C₁₃, C₁₁, and C₁₃), 134.5 (C₈ and C₈), 134.5 (C₉ and C₉), 142.4 (C₁₂ and C₁₂), 153.2 (C₄), 155.4 (C₂ and C₆).

1-Methyl-2,6-bis[2-(3-methylphenyl)ethenyl]pyridinium iodide (4)

Yellow powder; yield: 56%, m.p. 204.2–203.2 °C, Elem. Anal: Calcd. for $C_{24}H_{24}IN$ ($M_w = 453.36$ g mol⁻¹): C, 63.58; H, 5.34; N, 3.09%. Found: C, 64.10; H, 5.67; N, 3.60%; IR (KBr, cm⁻¹): 3041 (C–H), 2919 (=N⁺–CH₃), 2853 (C–H), 1607, 1566 (C=C), 1488 (C=C), 1459, 1331 (C–H), 1283, 1234 (C–N), 975 (=CH), 687 (C–H); ¹H-NMR (200 MHz, DMSO-*d*₆, δ/ppm): 2.37 (6H, *s*, –CH₃), 4.31 (3H, *s*,

=N⁺–CH₃), 7.30 (2H, *d*, *J* = 7.5 Hz, CH=CH), 7.40 (4H, *m*, CH=CH and C₆H₄); 7.62–7.70 (6H, *m*, C₆H₄ and pyridine), 8.29 (2H, *d*, *J* = 7.6 Hz, C₆H₄); 8.45 (1H, *d*, *J* = 6.4 Hz, pyridine); ¹³C-NMR (50 MHz, DMSO-*d*₆, δ/ppm): 21.7 (–CH₃), 40.2 (=N⁺–CH₃), 124.25 (C₇ and C₇), 128.3 (C₃ and C₅), 128.9 (C₁₀ and C₁₀), 129.2 (C₁₄ and C₁₄), 130.4 (C₁₂ and C₁₂), 131.5 (C₁₁ and C₁₁), 134.7 (C₈ and C₈), 137.3 (C₁₃ and C₁₃), 139.61 (C₉ and C₉), 153.1 (C₄), 155.2 (C₂ and C₆).

1-Methyl-2,6-bis[2-(3-hydroxyphenyl)ethenyl]pyridinium iodide (6)

Dark yellow powder; yield: 54%, m.p. 197.1–187 °C, Elem. Anal: Calcd. for $C_{22}H_{20}INO_2$ ($M_w = 457.30$ g mol⁻¹): C, 57.78; H, 4.41; N, 3.06%; Found: C, 57.33; H, 3.91; N, 3.54%; IR (KBr, cm⁻¹): 3320 (O–H stretching), 3045 (C–H), 2926 (=N⁺–CH₃), 2852 (C–H), 1608, 1570 (C=C), 1488 (C=C), 1265, 1235 (C–N), 1171 (C–O stretching), 965 (=CH), 790 (–CH); ¹H-NMR (200 MHz, DMSO-*d*₆, δ/ppm): 4.27 (3H, *s*, =N⁺–CH₃), 6.74 (2H, *d*, –OH), 7.10–7.18 (6H, *m*, C₆H₄ and CH₂=CH), 7.44 (2H, *d*, *J* = 7.4 Hz, CH=CH), 7.65 (4H, *m*, pyridine and C₆H₄), 7.88 (2H, *td*, *J* = 4.9 Hz, *J* = 4.5 Hz, C₆H₄), 8.26 (1H, *d*, *J* = 7.8 Hz, pyridine); ¹³C-NMR (50 MHz, DMSO-*d*₆, δ/ppm): 40.5 (=N⁺–CH₃), 113.89 (C₁₄ and C₁₄), 114.27 (C₁₂ and C₁₂), 119.74 (C₁₀ and C₁₀), 124.43 (C₇ and C₇), 128.24 (C₃ and C₅), 130.30 (C₁₁ and C₁₁), 139.12 (C₈ and C₈), 142.86 (C₉ and C₉), 153.52 (C₄), 158.09 (C₂ and C₆).

1-Methyl-2,6-bis[2-(4-fluorophenyl)ethenyl]pyridinium iodide (7)

Dark red crystals; yield: 57%, m.p. 213.5 °C, Elem. Anal: Calcd. for $C_{22}H_{18}F_2IN$ ($M_w = 461.29$ g mol⁻¹): C, 57.28; H, 3.93; N, 3.04%. Found: C, 57.68; H, 4.28; N, 3.24%; IR (KBr, cm⁻¹): 3077 (C–H), 2933 (=N⁺–CH₃), 2853 (C–H); 1560, 1595 (C=C), 1484 (C=C), 1288 (C–N), 1233, 1189 (C–F stretching); 971 (=CH); ¹H-NMR (200 MHz, DMSO-*d*₆, δ/ppm): 4.30 (3H, *s*, =N⁺–CH₃), 7.00 (2H, *d*, *J* = 8.8 Hz, CH=CH), 7.36–7.71 (4H, *m*, CH=CH, and pyridine), 7.93 (4H, *t*, *J* = 7.0 Hz, C₆H₄), 8.09–8.28 (4H, *m*, C₆H₄), 8.44 (1H, *dd*, *J* = 7.9, *J* = 4.4 Hz, pyridine); ¹³C-NMR (50 MHz, DMSO-*d*₆, δ/ppm): 48.32 (=N⁺–CH₃), 115.11 (C₁₁, C₁₃, C₁₀, and C₁₃), 124.28 (C₇ and C₇), 130.86 (C₃ and C₅), 131.42 (C₁₀, C₁₄, C₁₀, and C₁₄), 133.73 (C₉ and C₉), 140.59 (C₈ and C₈), 143.56 (C₄), 153.48 (C₂ and C₆), 155.57 (C₁₂ and C₁₂).

1-Methyl-2,6-bis[2-(4-chlorophenyl)ethenyl]pyridinium iodide (8)

Yellow powder; yield: 61%, m.p. 208 °C, Elem. Anal: Calcd. for $C_{22}H_{18}Cl_2IN$ ($M_w = 494.20$ g mol⁻¹): C, 53.47;

H, 3.67; N, 2.83%. Found: C, 53.70; H, 3.32; N, 2.59%; IR (KBr, cm^{-1}): 3026 (C–H), 2929 ($=\text{N}^+-\text{CH}_3$), 2858 (C–H); 1622, 1564 (C=C), 1487 (C=C), 1280, 1248 (C–N), 1081 (C–Cl stretching), 971 ($=\text{CH}$); $^1\text{H-NMR}$ (200 MHz, $\text{DMSO-}d_6$, δ/ppm): 40.30 (3H, *s*, $=\text{N}^+-\text{CH}_3$), 7.02 (2H, *d*, $J=7.7$ Hz, $\text{CH}=\text{CH}$); 7.26–7.52 (4H, *m*, $\text{CH}=\text{CH}$ and pyridine), 7.73 (4H, *d*, $J=7.2$ Hz, C_6H_4), 8.05–8.18 (4H, *m*, C_6H_4), 8.45 (1H, *dd*, $J=8.1$ Hz, $J=5.5$ Hz, pyridine); $^{13}\text{C-NMR}$ (50 MHz, $\text{DMSO-}d_6$, δ/ppm): 48.30 ($=\text{N}^+-\text{CH}_3$), 124.31 (C_7 and C_7), 128.80 (C_{11} , C_{13} , C_{11} , and C_{13}), 130.42 (C_{10} , C_{14} , C_{10} , and C_{14}), 131.01 (C_3 and C_5), 135.6 (C_9 and C_9), 138.2 (C_8 and C_8), 144.58 (C_4), 145.57 (C_{12} and C_{12}), 154.50 (C_2 and C_6).

1-Methyl-2,6-bis[2-(2,6-dichlorophenyl)ethenyl]pyridinium iodide (9)

Yellow powder; yield: 45%, m.p. 204.1–203.7 °C, Elem. Anal. Calcd. for $\text{C}_{22}\text{H}_{16}\text{Cl}_4\text{IN}$ ($M_w = 563.09$ g mol^{-1}): C, 46.93; H, 2.86; N, 2.49; %, Found: C, 46.43; H, 2.41; N, 2.29%; IR (KBr, cm^{-1}): 3038 (C–H), 2929 ($=\text{N}^+-\text{CH}_3$), 2852 (C–H), 1615, 1575 (C=C), 1481 (C=C), 1268 (C–N), 1075 (C–Cl), 964 ($=\text{CH}$); $^1\text{H-NMR}$ (200 MHz, $\text{DMSO-}d_6$, δ/ppm): 4.24 (3H, *s*, $=\text{N}^+-\text{CH}_3$), 7.47–7.52 (4H, *m*, $\text{CH}=\text{CH}$ and pyridine), 7.61 (2H, *d*, $J=4.1$ Hz, $\text{CH}=\text{CH}$), 7.62–7.69 (4H, *m*, $-\text{C}_6\text{H}_3$), 8.33–8.37 (2H, *d*, $J=8.1$ Hz, $-\text{C}_6\text{H}_3$), 8.60 (1H, *m*, pyridine); $^{13}\text{C-NMR}$ (50 MHz, $\text{DMSO-}d_6$, δ/ppm): 42.82 ($=\text{N}^+-\text{CH}_3$), 126.16 (C_7 and C_7), 128.61 (C_3 and C_5), 129.43 (C_{11} , C_{13} , C_{11} , and C_{13}), 131.56 (C_{12} and C_{12}), 134.12 (C_{10} , C_{14} , C_{10} , and C_{14}), 136.48 (C_8 and C_8), 145.16 (C_9 and C_9), 152.87 (C_4), 156.47 (C_2 and C_6).

1-Methyl-2,6-bis[2-(2-chloro-6-fluorophenyl)ethenyl]pyridinium iodide (10)

Black crystals; yield: 44%, m.p. 170 °C, Elem. Anal. Calcd. for $\text{C}_{22}\text{H}_{16}\text{Cl}_2\text{F}_2\text{IN}$ ($M_w = 530.18$ g mol^{-1}): C, 49.84; H, 3.04; N, 2.64%; Found: C, 49.62; H, 3.34; N, 3.14%; IR (KBr, cm^{-1}): 3072 (C–H), 2929 ($=\text{N}^+-\text{CH}_3$), 2853 (C–H), 1603, 1576 (C=C), 1486 (C=C), 1242 (C–N), 1172 (C–F), 1062 (C–Cl), 977 ($=\text{CH}$); $^1\text{H-NMR}$ (200 MHz, $\text{DMSO-}d_6$, δ/ppm): 4.26 (3H, *s*, $=\text{N}^+-\text{CH}_3$), 7.49–7.56 (4H, *m*, $\text{CH}=\text{CH}$ and pyridine), 7.60 (2H, *d*, $J=4.7$ Hz, C_6H_3), 7.64–7.94 (6H, *m*, pyridine, C_6H_3 and $\text{CH}=\text{CH}$), 7.99 (2H, *d*, $J=8.1$ Hz, C_6H_3), 8.60 (1H, *m*, pyridine); $^{13}\text{C-NMR}$ (50 MHz, $\text{DMSO-}d_6$, δ/ppm): 45.20 ($=\text{N}^+-\text{CH}_3$), 115.51 (C_{13} and C_{13}), 128.12 (C_7 and C_7), 129.51 (C_3 and C_5), 130.5 (C_{11} and C_{11}), 134.22 (C_{10} and C_{10}), 145.5 (C_9 and C_9), 137.9 (C_8 and C_8), 150.08 (C_4), 153.62 (C_2), 160.22 (C_{14} and C_{14}).

1-Methyl-2,6-bis[2-(4-nitrophenyl)ethenyl]pyridinium iodide (12)

Black crystals; yield: 61%, m.p. 204.2–203.2 °C, Elem. Anal. Calcd. for $\text{C}_{22}\text{H}_{18}\text{IN}_3\text{O}_4$ ($M_w = 515.30$ g mol^{-1}): C, 51.28; H, 3.52; N, 8.15%; Found: C, 51.70; H, 3.84; N, 7.85%; IR (KBr, cm^{-1}): 3002 (C–H), 2921 ($=\text{N}^+-\text{CH}_3$), 2853 (C–H); 1624, 1519 (C=C), 1490 (C=C), 1280 (C–N), 1345 (N–O stretching of $-\text{NO}_2$ group); 971 ($=\text{CH}$); $^1\text{H-NMR}$ (200 MHz, $\text{DMSO-}d_6$, δ/ppm): 4.30 (3H, *s*, $=\text{N}^+-\text{CH}_3$); 7.20–7.52 (4H, *m*, $\text{CH}=\text{CH}$ and pyridine), 7.60 (2H, *d*, $J=6.8$ Hz, $\text{CH}=\text{CH}$), 8.20 (4H, *d*, $J=7.4$ Hz, C_6H_4), 8.36 (4H, *d*, $J=7.4$ Hz, C_6H_4), 8.57–8.62 (1H, *br.m.ovlp*, pyridine); $^{13}\text{C-NMR}$ (50 MHz, $\text{DMSO-}d_6$, δ/ppm): 42.3 ($=\text{N}^+-\text{CH}_3$), 124.2 (C_{11} , C_{13} , C_{110} , and C_{13}), 124.6 (C_7 and C_7), 126.9 (C_3 and C_5), 125.6 (C_{10} , C_{14} , C_{10} , and C_{14}), 137.8 (C_9 and C_9), 139.5 (C_8 and C_8), 144.9 (C_{12} and C_{12}), 155.2 (C_4), 157.5 (C_2 and C_6).

1-Methyl-2,6-bis[2-(4-methoxyphenyl)ethenyl]pyridinium iodide (13)

Yellow powder; yield: 59%, m.p. 207.8 °C, Elem. Anal. Calcd. for $\text{C}_{24}\text{H}_{24}\text{INO}_2$ ($M_w = 485.36$ g mol^{-1}): C, 59.39; H, 4.98; N, 2.89%; Found: C, 59.63; H, 5.21; N, 2.60%; IR (KBr, cm^{-1}): 3046 (C–H), 2936 ($=\text{N}^+-\text{CH}_3$), 2833 (C–H stretching of $-\text{CH}_3$ group attached to nitrogen and oxygen), 1599, 1560 (C=C); 1484 (C=C), 1325, 1254 (C–N), 1175 (C–O asymmetric stretching of $-\text{OCH}_3$ group), 1023 (C–O stretching of $-\text{OCH}_3$ group), 978 ($=\text{CH}$); $^1\text{H-NMR}$ (200 MHz, $\text{DMSO-}d_6$, δ/ppm): 3.84 (6H, *s*, $-\text{OCH}_3$), 4.26 (3H, *s*, $=\text{N}^+-\text{CH}_3$), 6.81 (4H, *d*, $J=7.8$ Hz, C_6H_4), 7.06 (2H, *d*, $J=8.4$ Hz, $\text{CH}=\text{CH}$), 7.51 (2H, *d*, $J=8.4$ Hz, $\text{CH}=\text{CH}$), 7.79 (2H, *dd*, $J=7.5$ Hz, $J=4.8$ Hz, pyridine), 8.22 (4H, *d*, $J=7.8$ Hz, C_6H_4), 8.34–8.37 (1H, *m*, pyridine); $^{13}\text{C-NMR}$ (50 MHz, $\text{DMSO-}d_6$, δ/ppm): 43.1 ($=\text{N}^+-\text{CH}_3$), 55.3 ($-\text{OCH}_3$), 114.1 (C_{11} , C_{13} , C_{11} , and C_{13}), 126.3 (C_7 and C_7), 128.4 (C_3 and C_5), 139.2 (C_{10} , C_{14} , C_{10} , and C_{14}), 140.1 (C_9 and C_9), 141.93 (C_8 and C_8), 152.7 (C_4), 153.84 (C_2 and C_6), 159.8 (C_{12} and C_{12}).

1-Methyl-2,6-bis[2-(3,4-dimethoxyphenyl)ethenyl]pyridinium iodide (14)

Orange powder; yield: 58%, m.p. 235 °C, Elem. Anal. Calcd. for $\text{C}_{26}\text{H}_{28}\text{INO}_4$ ($M_w = 545.41$ g mol^{-1}): C, 57.26; H, 5.17; N, 2.57%; Found: C, 57.61; H, 4.89; N, 3.01%; IR (KBr, cm^{-1}): 3045 (C–H), 2925 ($=\text{N}^+-\text{CH}_3$), 2852 (C–H), 1599, 1561 (C=C), 1484 (C=C), 1357, 1322 (C–N), 1273, 1249 (C–O), 1016 (C–O), 965 ($=\text{CH}$); $^1\text{H-NMR}$ (200 MHz, $\text{DMSO-}d_6$, δ/ppm): 3.85 (12H, *s*, $J=7.4$ Hz, $-\text{OCH}_3$), 4.29 (3H, *s*, $=\text{N}^+-\text{CH}_3$), 7.07 (2H, *d*, $J=8.4$ Hz, C_6H_4), 7.40 (2H, *d*, $\text{CH}=\text{CH}$ and pyridine), 7.49–7.68 (6H, *m*, $J=8.4$ Hz, C_6H_4 ,

pyridine and CH=CH), 8.21 (2H, *d*, $J=7.9$ Hz, C₆H₄); 8.38 (1H, *t*, $J=7.1$ Hz, pyridine); ¹³C-NMR (50 MHz, DMSO-*d*₆, δ /ppm): 43.2 (=N⁺-CH₃), 56.40 (-OCH₃), 60.71 (-OCH₃), 110.71 (C₁₄ and C₁₄), 114.14 (C₁₁ and C₁₁), 119.74 (C₃ and C₃), 122.79 (C₁₀ and C₁₀), 126.40 (C₇ and C₇), 136.79 (C₄), 140.8 (C₉ and C₉), 141.40 (C₈ and C₈), 153.61 (C₂ and C₆), 155.68 (C₁₂ and C₁₂), 159.79 (C₁₃ and C₁₃).

1-Methyl-2,6-bis[2-(3,4,5-trimethoxyphenyl)ethenyl]pyridinium iodide (15)

Orange crystals; yield: 61%, m.p. 236 °C, Elem. Anal. Calcd. for C₂₆H₂₈INO₄ ($M_w=605.46$ g mol⁻¹): C, 55.54; H, 5.33; N, 2.31; %, Found: C,55.21; H, 5.83; N, 2.73%; IR (KBr, cm⁻¹): 3045 (C-H), 2935 (=N⁺-CH₃), 2833 (C-H), 1596, 1568 (C=C), 1484 (C=C), 1345, 1326 (C-N), 1247, 1122, (C-O), 1020 (C-O), 964 (=CH); ¹H-NMR (200 MHz, DMSO-*d*₆, δ /ppm): 3.86 (18H, *d*, $J=7.4$ Hz, -OCH₃), 4.30 (3H, *s*, =N⁺-CH₃), 7.08 (2H, *d*, $J=8.4$ Hz, C₆H₄), 7.40–7.43 (4H, *m*, CH=CH and Py), 7.49–7.68 (6H, *m*, $J=8.4$ Hz, C₆H₄, pyridine and CH=CH), 8.21 (2H, *d*, $J=7.9$ Hz, C₆H₄), 8.38 (1H, *br.m.ovlp*, pyridine); ¹³C-NMR (50 MHz, DMSO-*d*₆, δ /ppm): 43.2 (=N⁺-CH₃), 56.20 (-OCH₃), 60.90 (-OCH₃), 73.22 (-OCH₃), 105.4 (C₁₄ and C₁₄), 106.80 (C₁₀ and C₁₀), 113.8 (C₁₁ and C₁₁), 119.85 (C₃ and C₃), 126.35 (C₇ and C₇), 140.65 (C₈ and C₈), 141.15 (C₉ and C₉), 136.45 (C₄), 153.8 (C₂ and C₆), 145.6 (C₁₂ and C₁₂), 156.1 (C₁₃ and C₁₃).

Molecular geometry optimization and theoretical absorption spectra calculation

The ground state geometries of isomers, i.e., *s-trans/s-trans* and *s-cis/s-cis*, (explanation for conformers naming is given in previous paper [13]) of compounds **1–15** (considered as cations) were optimized in gas phase with the DFT method. Halogen anions were not included in computational considerations in this work. First, the conformational search for every isomer was conducted by varying C7–C8–C9–C10 torsional angle from 0° to 180° by 20° increment and fully optimizing the structure using B3LYP method with Def-2SVP basis set. After that, conformer with the lowest energy was re-optimized using the same functional but with larger Def2TZVP basis set [21]. Global minima were found for each optimized compound and confirmed by calculations of harmonic vibrational frequencies (no imaginary frequency were found). Theoretical absorption spectra were calculated in DMSO solution with the TD-DFT method, more specifically with CAM-B3LYP long range corrected functional,[22] and Def2TZVP basis set on gas phase optimized geometries. Solvent in the TD-DFT calculations was simulated with standard polarized continuum model (PCM) [23]. Occupations of valence anti-bonding (π^*) and bonding (π)

orbitals of partial double bonds were theoretically calculated with the B3LYP/Def2TZVP wave function, using natural bond orbital (NBO) [24] population analysis for electron localization procedure. All quantum chemical calculations were done in Gaussian09 [25] program package.

LSER and LFER analysis

The non-specific solvent effect, i.e., solvent dipolarity/polarizability, and specific ones, i.e., solvent–solute hydrogen bonding interactions, were evaluated by means of the LSER models in first instance applying the Kamlet–Taft equation [26]:

$$\nu_{\max} = \nu_o + s\pi^* + b\beta + a\alpha \quad (1)$$

where ν_{\max} is the absorption frequency maxima; π^* is an index of the solvent dipolarity/polarizability; β is a measure of the solvent hydrogen-bond acceptor (HBA) basicity; α is a measure of the solvent hydrogen-bond donor (HBD) acidity, and ν_o is the regression value in cyclohexane as a reference solvent. The regression coefficients s , b , and a in Eq. (1) represents measure of the relative susceptibilities of the absorption frequencies to the solvent effect. The solvent parameters used in Eq. (1) are given in Table S1.

To obtain more specific separation of solvent effects the Catalán equation was used [27]:

$$\nu_{\max} = \nu_o + cSP + dSdP + bSB + aSA \quad (2)$$

where SP, SdP, SA, and SB characterize solvent polarizability, dipolarity, basicity, and acidity, respectively; and $a-d$ are the regression coefficients describing the sensitivity of the absorption maxima to the different types of the solvent–solute interactions. The solvent parameters used in Eq. (2) are given in Table S2. Separation of non-specific solvent effects, term π^* in Eq. (1), into two terms: dipolarity and polarizability, SP and SdP in Eq. (2), contributes to the advantageous analysis of the solvatochromism of the studied compounds.

NMR chemical shifts were subjected to the linear free energy relationship analysis (LFER). The transmission of substituent effects was studied using single substituent parameter equation (SSP) in the form:

$$S = \rho\sigma + h \quad (3)$$

where S is a substituent–dependent value: absorption frequencies (ν_{\max}) or NMR chemical shifts; ρ is the proportionality constant reflecting the sensitivity of the chemical shifts spectral data to the substituent effects, σ is the corresponding substituent constant, and h is the intercept (i.e., describes the unsubstituted member of the series) [28]. The substituent parameters used in Eq. (3) are given in Table S3, where σ values correspond to an additive blend of polar and π -delocalization effects.

Regression and correlation

The dependence of the parameter solvents and absorption frequencies were interpreted using multiple linear regression analysis. All correlations were performed at the 95% confidence level. The quality of the correlation model was shown through the value of the correlation coefficient, standard error and the Fisher's test (F).

Antioxidant activity

Antioxidant activity was determined using 1,1-diphenyl-2-picrylhydrazyl (DPPH) and 2,2'-azino-bis(3-ethylbenzothiazoline-6-sulfonic acid) (ABTS) radical scavengers.

DPPH method

Test solutions were prepared by dissolving ten different amounts of compound in methyl alcohol. Commercially available DPPH radical was dissolved in methanol at concentration of $5.34 \times 10^{-5} \text{ mol L}^{-1}$. A 96-well microplate was loaded with 140 μL of DPPH solution and 10 μL of test solution or pure methanol as the control. The microplate was incubated for 30 min at room temperature in the dark. After incubation, absorbance of DPPH radical was measured at 517 nm using a Thermo Scientific Appliskan. All the measurements were carried out in triplicate. The scavenging activity was calculated using equation Eq. (4):

$$\% \text{DPPH radical scavenging activity} = \left((A_{\text{control}} - A_{\text{sample}}) / A_{\text{control}} \right) \times 100 \quad (4)$$

where A_{sample} and A_{control} refer to the absorbances at 517 nm of DPPH in the sample and control solutions, respectively. Ascorbic acid was used as the reference compound.

ABTS method

ABTS solution was prepared by dissolving 19.2 mg of ABTS in 5 mL of $\text{K}_2\text{S}_2\text{O}_8$ solution (33 mg $\text{K}_2\text{S}_2\text{O}_8$ in 50 mL H_2O) and diluting with methanol to obtained absorbance of 0.700 ± 0.020 at 734 nm. Experiments were performed on the UV/Vis spectrophotometer. The reaction mixture is consisted of 2.8 mL of ABTS radical solution and 0.2 mL of tested compound solution in methanol (total volume, 3 mL). After incubation in the dark for 20 min, the absorbance was recorded at 734 nm. As a control, solution of ABTS in methanol (2.8 mL of ABTS and 0.2 mL methanol) was used. Ascorbic acid was used as a reference. The scavenging activity was calculated using equation Eq. (5):

$$\% \text{ABTS radical scavenging activity} = \left(1 - (A_{\text{sample}} / A_{\text{control}}) \right) \times 100 \quad (5)$$

where A_{sample} and A_{control} refer to the absorbances at 734 nm of ABTS in the sample and control solutions, respectively.

Results and discussion

Chemistry

The investigated compounds were synthesized by condensation of 1-methyl-2,6-dimethylpyridinium iodide and appropriate aldehyde (Scheme 1). Chemical structures of the synthesized compounds **1–15** were confirmed using IR and NMR spectroscopy, and the purity was verified by the melting point determination and elemental analysis. Due to a well-known fact about possibility of rotational isomerism around ethylenic bond it was necessary to perform molecular geometry optimization taking into account all possible rotational isomers and stepwise procedure to obtain structure with the lowest energy.

Geometry optimization and TD-DFT calculations

The investigated compounds contain two symmetric substituted aryl rings attached to the central pyridine ring by ethylenic bridging group. The physico-chemical properties of these compounds are determined by either existence of dominant conformational species or the dynamic equilibrium between the isomers. The inter-conversion between possible rotational isomers occurs by the rotation of the arylvinyl moieties around the quasi-single bonds with the central pyridine through the thermal or photochemical processes [29]. The state of the *s-cis/s-cis* and *s-trans/s-trans* forms equilibria in solvents of different polarity depends on the energy of the appropriate form, activation energy necessary for inter-conversion or type and strength of the solute/solvent interactions. It has been previously published that, in the solid state, preferred conformation of compound is determined by the magnitude of weak steric interactions between two vinyl hydrogen atoms and one found at lower distance on pyridyl ring. This can, also, be of appropriate significance in the solution [30].

Results of the electronic energy calculations on the most stable geometry of both isomers, performed at B3LYP/Def2TZVP level, are given in Table 1. Structures and elements of the optimized geometries are shown in Fig. 1 and Table S4, respectively.

Energies of the optimized structures in gas phase (Table 1) indicate dominant presence of the *s-trans/s-trans* form of all synthesized derivatives, which is in consistence with the reported crystallographic data of the most stable conformation of similar compounds [31]. According to the geometry optimization results for 4-hydroxy substituted molecule (**5**), obtained using DGDZVP basis set, *s-cis/s-trans*

Table 1 Energies of optimized structure of studied compounds 1–15

Comp.	Energy (hartrees) (B3LYP/Def2TZVP)		ΔE (kcal mol ⁻¹)
	<i>s-trans/s-trans</i> isomer	<i>s-cis/s-cis</i> isomer	
1	-905.23742	-905.22834	-5.70
2	-1212.63497	-1212.62578	-5.77
3	-983.90554	-983.89653	-5.65
4	-983.90280	-983.89390	-5.58
5	-1055.75594	-1055.74715	-5.51
6	-1055.74958	-1055.74088	-5.46
7	-1103.79731	-1103.78806	-5.80
8	-1824.48456	-1824.47538	-5.76
9	-2743.71593	-2743.70593	-6.28
10	-2023.03443	-2023.02504	-5.89
11	-1173.29633	-1173.28752	-5.53
12	-1314.39540	-1314.38607	-5.86
13	-1134.38775	-1134.37902	-5.48
14	-1363.50965	-1363.50185	-4.90
15	-1592.63340	-1592.62566	-4.86

Only structure of cation was considered (counter ion was excluded from calculation)

conformation has been found as the most stable [13]. However, the basis set used in the mentioned work differs from the basis set used in the present work, and thus the results are not comparable.

Depending on the type and number of the groups attached to the two symmetric benzene rings bonds length and the geometrical arrangement vary among the synthesized derivatives. Bond distances and angles, defined by the numbering according to the Scheme 1 and S2, and the sizes of dihedral angles of interest, presented in Fig. 2, are given in Table S4.

The influence of the substituents on the C₁–N₁ bond length is negligible for the electron-accepting groups while the electron-donating groups, especially the strongest N(CH₃)₂, cause decrease in this bond length. The most prominent substituent effect can be observed on the lengths of C₂–C₇–C₈–C₉ and C₆–C₇′–C₈′–C₉′ unsaturated bonds (Schemes 1 and S2). Electron-donating groups cause decrease in the C₂–C₇ (C₆–C₇′) and C₈–C₉ (C₈′–C₉′) bonds length (except ones in *m*-position), while opposite is true for the electron-acceptor substituted compounds. The influence is slightly more noticeable on the C₈–C₉ (C₈′–C₉′) bonds due to the proximity of the substituent. Electron donors in the *para*-position have the strongest impact on the bond length decrease due to high contribution of extended π -electron delocalization. The smaller influence of the electron-donating group in the *ortho*-position is related to the steric hindrance, so called *ortho*-effect, which can cause modification of the extent of π -electron delocalization. On the contrary, electron-accepting groups increase the length of those four bonds with the exception of halogens in the *p*-position. Most

likely, due to competitive positive resonance and negative inductive effect of halogen atoms bond lengths remain similar as one found in the unsubstituted molecule. Conversely, length of C₇=C₈ (C₇′=C₈′) double bonds decreases with electron accepting, and increases with electron-donating groups. In general, the largest decrease and increase of the bond lengths is found in compounds with the strongest electron-accepting group, i.e., NO₂ group, and the strongest electron-donating group, i.e., N(CH₃)₂ group, respectively.

In addition, compared to the unsubstituted compound (1), bond angles vary in different derivatives. As can be seen in Table S4, halogens in the *ortho*-position have the most prominent influence on the angles. This can be related to the specific 4nature (balanced contribution of both +R and –I effects with additional *ortho*-effect) and the small voluminosity of the halogens, especially fluorine. These effects cause appropriate geometry adjustment as a response to the electronic demands of the environment. These effects cause appropriate geometry adjustment as a response to the electronic demands of the environment. From the values of dihedral angles (Table S4) it can be seen that deviation of the planarity increases with the increase of the electron-accepting ability of the substituents, while the derivative with the strongest electron-donating group shows higher planarity.

Solvatochromism of the studied compounds: multi-parameter correlations

LSER analysis is frequently used as core concept of predictive analysis related to study of the relationship between the structure and properties of the investigated molecules. With the aid of theoretical absorption spectra, behavior of the studied compounds can be described by electronic structure in both, ground and excited states induced by the change of the solvent properties. Results of DFT calculations on the stability of theoretically possible isomers show that *s-trans/s-trans* form dominates in both, gas phase and solution. Because the energy necessary for the effective rotation is much higher than the thermal energy of the isomeric forms, *s-trans/s-trans* isomer is dominant in the solution. Similar results related to the structure of absorption bands in systems with the ethylenic bridge in the *ortho*-position with respect to the nitrogen heteroatom of central pyridine ring have, already, been obtained as a result of the influence of double bond [16]. Their common characteristic is the presence of a strong absorption band in the 350–450 nm range that originates from the *s-trans* isomer. Bands of medium intensity are also present at a shorter wavelength (275–315 nm), and are ascribed to the *cis*-rotamer [32].

The absorption spectra, recorded in 20 solvents, are complex and show presence of 2 or 3, not well separated, electronic transitions. Examples of the spectra of all compounds in four solvents are given in Fig. 3. Intensity and absorption

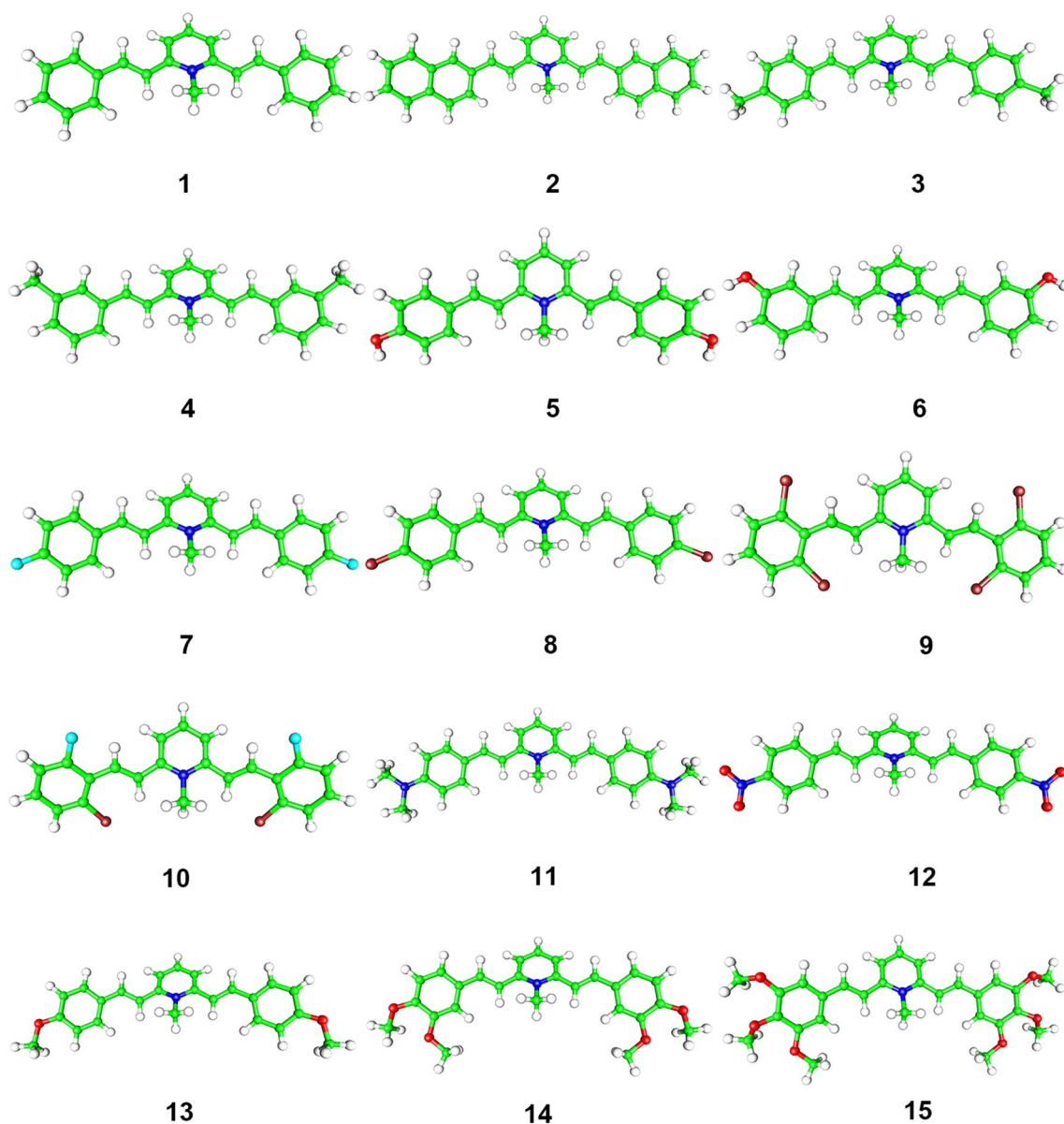


Fig. 1 Optimized geometries of the most stable *s-trans/s-trans* conformations of compounds 1–15 in DMSO

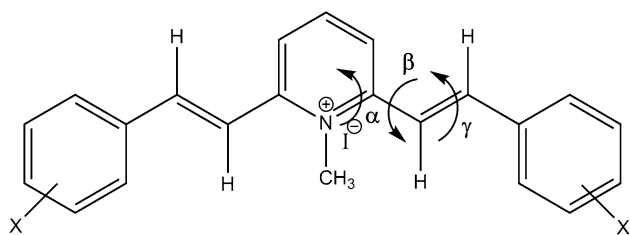


Fig. 2 Dihedral angles used in conformational analysis of investigated compounds

frequencies of the main absorption bands (Table S5) depend on the electronic structure of the studied compounds and the solvent properties. In general, compared to the compound **1**, in all used solvents, electron-donating groups cause increase in π -conjugation and induce bathochromic shift, due to more effective π -electronic transfer through substituted styryl moieties, while the opposite effect is noticed for the electron-acceptors [33].

As described by Wang et al. [18], absorption and emission maxima of *N*-methyl-2,3-distyryl-pyridine are strikingly red shifted upon methylation which creates cross-conjugated system, very similar to cyanine array. Analysis of the substituent effect on the disturbance/enhancement of

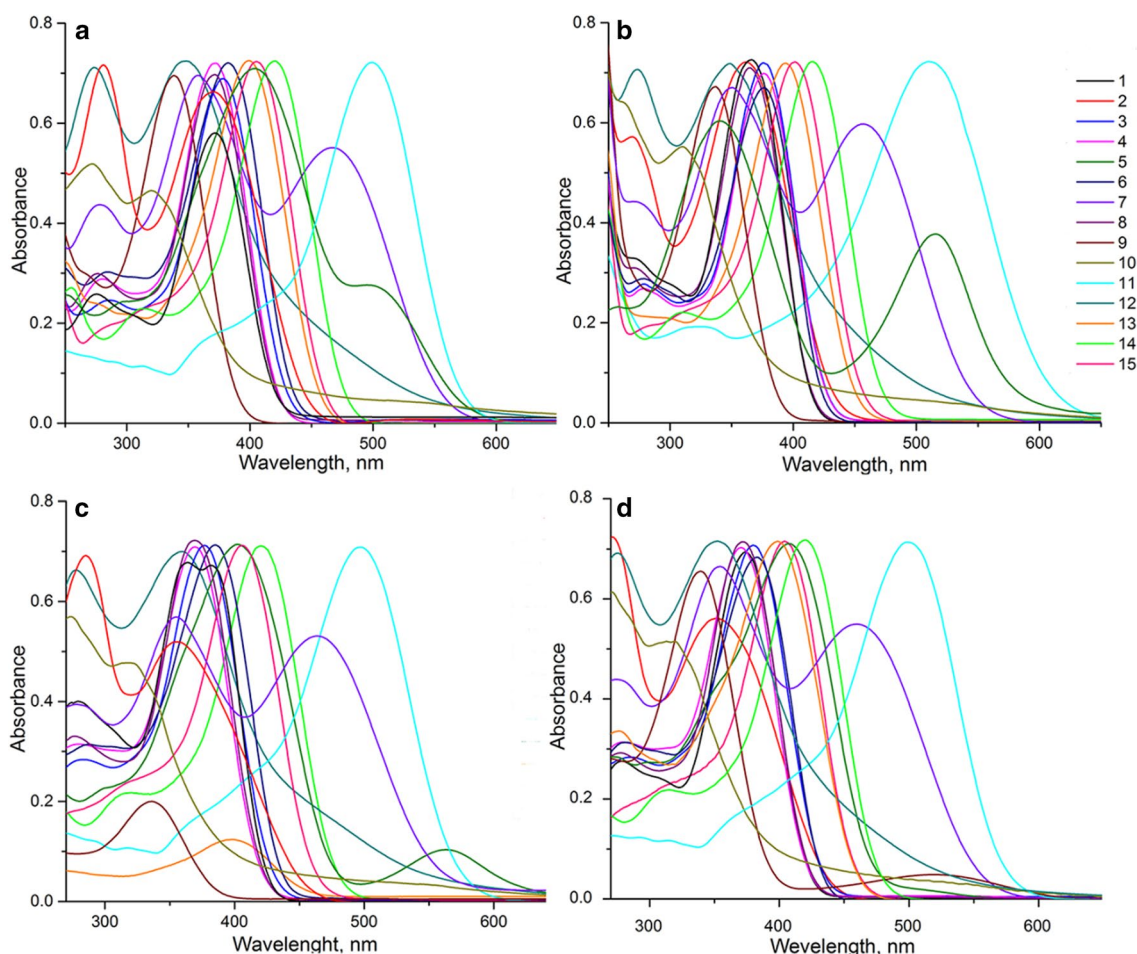


Fig. 3 Absorption spectra of compounds **1–15** in **a** EtOH, **b** AcN, **c** DMSO, and **d** F

π -electron delocalization in studied compounds is in accordance with the known fact that increased electron conjugation produces larger bathochromic shift. Derivatives with electron-donating group in *p*-position support effective π -electron conjugation and, thus they show larger bathochromic shift. Presence of methyl group in the *m*-position disturbs the conjugation, and, compared to compound **1**, compound **4** shows hypsochromic shift. Considering the magnitude of the ν_{\max} shift of *p*-OH substituted derivatives it can be seen that more polar solvents produce larger bathochromic shift. The effect of substituent position can be explained by comparing solvatochromic behavior of the compounds **13–15** on one side, and **9** and **10** on the other. UV–Vis spectra of the compounds **13–15** (mono, di, and three substituted derivatives with electron-donating methoxy group) are red shifted in comparison to the compound **1**. It is expected that compound **15**, with three strong electron-donating groups, shows the largest shift. However, cross-effect of two *meta* and one *para* methoxy groups contributes to lower π -electron delocalization and thus lowers red shift compared to the compound **14**. On the other hand, compared to the derivative

12 (the strongest electron-accepting group), compounds **9** and **10** show larger hypsochromic effect. Halogen atoms show complex influence due to position-dependent contribution of positive resonance and negative inductive effect, and also steric interference of atom in the *ortho*-position. Moreover, as expected for compound **11** (the strongest electron-accepting substituent) additional red shift of peak at $\nu_{\max} = 20.34 \text{ cm}^{-1}$ compared to the other compounds suggests more pronounced ICT interaction in the molecule.

LSER analysis: correlation with multi-parameter solvent polarity scales

The position, intensity, and shape of bands in the absorption spectra depend on the solvent properties. Multi-parameter approach is often used to describe/evaluate the influence of solvent effects on the absorption maxima change. The interactions between solute and solvent molecules have been quantified using Kamlet–Taft and Catalán LSER models. The correlation coefficient (R), the standard error of the estimate (sd), Fisher's significance test (F), regression values ν_0 ,

Table 2 Results of the correlations for compounds **1–15** obtained according to Kamlet–Taft equation

Comp.	$\nu_0 \times 10^{-3} (\text{cm}^{-1})$	$s \times 10^{-3} (\text{cm}^{-1})$	$b \times 10^{-3} (\text{cm}^{-1})$	$a \times 10^{-3} (\text{cm}^{-1})$	R^a	Sd^b	F^c	Solvent excluded from the correlation
1	25.19 ± 0.19	0.90 ± 0.1	0.95 ± 0.20	0.34 ± 0.09	0.93	0.11	20.94	THF, acetone, TCM, AcN, anisole, NMF
2	26.45 ± 0.20	0.18 ± 0.21	0.72 ± 0.18	0.55 ± 0.12	0.93	0.14	21.08	Acetone, EtOAc, DMF, DMSO, EtOH, dioxane
3	26.41 ± 0.08	0.10 ± 0.08	0.17 ± 0.09	-0.40 ± 0.04	0.96	0.05	42.89	Anisole, TCM, <i>t</i> -AmOH, THF
4	27.44 ± 0.08	-0.11 ± 0.07	-0.34 ± 0.08	-0.28 ± 0.04	0.94	0.06	31.41	Anisole, TCM, THF, DMF
5	27.26 ± 0.33	-0.78 ± 0.33	-2.21 ± 0.27	-0.72 ± 0.18	0.95	0.22	34.68	EtAc, THF, dioxane, 2-PrOH, AcN
6	27.04 ± 0.15	-0.31 ± 0.16	-1.41 ± 0.14	0.27 ± 0.09	0.95	0.11	32.81	EtAc, THF, DMSO, DMA, anisole, 1-PrOH
7	22.03 ± 0.11	0.28 ± 0.11	-0.90 ± 0.14	-0.19 ± 0.06	0.95	0.08	33.09	Anisole, acetone, TCM, <i>t</i> -Amylol, 2-PrOH
8	26.81 ± 0.11	-0.17 ± 0.13	-0.22 ± 0.11	0.48 ± 0.07	0.93	0.08	24.90	DMF, DMSO, <i>t</i> -amylol, AcN, NMF
9	29.84 ± 0.07	-0.14 ± 0.08	-0.12 ± 0.07	-0.29 ± 0.05	0.93	0.05	20.21	<i>i</i> PrOH, NMF, MeOH, <i>t</i> -AmOH anisole, THF
10	28.26 ± 0.31	-1.17 ± 0.59	0.75 ± 0.54	-0.69 ± 0.22	0.93	0.23	19.90	<i>t</i> -AmOH, NMF, acetone, MeOH, THF, DMA
11	20.15 ± 0.20	0.44 ± 0.20	-0.69 ± 0.23	-0.54 ± 0.13	0.94	0.14	23.39	<i>i</i> BuOH, <i>t</i> -AmOH, anisole, DMSO, F, DMA, NMF
12	28.93 ± 0.28	-1.60 ± 0.39	-0.17 ± 0.24	0.69 ± 0.15	0.95	0.14	28.20	<i>i</i> BuOH, <i>t</i> -AmOH, anisole, DMSO, F, DMA, NMF
13	25.38 ± 0.12	-0.94 ± 0.15	0.77 ± 0.13	-0.36 ± 0.08	0.94	0.09	20.92	F, <i>i</i> PrOH, AcN, dioxane, DMA, NMP
14	22.14 ± 0.20	0.42 ± 0.19	0.13 ± 0.18	0.10 ± 0.11	0.93	0.13	14.16	Dioxane, EtAc, acetone, AcN, anisole, DMSO, <i>i</i> PrOH
15	23.90 ± 0.08	0.48 ± 0.09	0.40 ± 0.08	0.21 ± 0.05	0.93	0.06	25.28	Dioxane, EtAc, NMF, DMA

^aCorrelation coefficient^bStandard deviation^cFisher's test of significance

s, *a*, and *b* (Kamlet–Taft), and *c*, *d*, *a*, and *b* (Catalán) are presented in Tables 2 and 3, respectively. Statistical analysis from multi linear analysis shows that both equations, i.e., Kamlet–Taft and Catalán, could be used successfully in LSER analysis of investigated symmetrical compound.

Large diversity of correlation results, related to the sign and values of solvatochromic parameters given in Table 2, indicate that both, solvent and substituent effects determine the position of UV maxima shifts. Negative sign of coefficient *s*, observed for compounds **4–6**, **8–10**, and **13**, indicates bathochromic (red) shift with increasing solvent dipolarity/polarizability. A hypsochromic shift (positive *s* coefficient), observed for others compounds, suggests better stabilization of excited state relative to ground state. Strong electron-accepting effect of nitro group contributes to larger stabilization of dipolar structure in excited state. Similar results found for compound **10** reflect synergetic influence of electron-accepting/resonance ability of *F* atom and steric effect of both substituents to larger stabilization of excited state. Otherwise, solvent effects on ν_{max} change for compounds with electron donor, i.e., hydroxy substituted compounds **5** and **6**, contribute to larger stabilization of excited state. Such behavior, also observed, earlier, for similar compounds [13], has been assumed to originate from the high symmetry of

the investigated compounds. In addition, synthesized compounds contain no lone electron pair at the pyridine nitrogen capable for proton accepting interaction with solvent. However, HBD solvents can be achieved through interactions with the oxygen or nitrogen from the substituent. According to the similarity of the values of coefficient *a* diversity of the stabilization of either ground state (compounds **1**, **2**, **6**, **8**, **12**, **14**, and **15**) or excited state found for other ones is found. Such specific solvent effect largely depends on hydrogen bonding ability of appropriate sites of investigated compounds and their conformational arrangement.

The highest values of coefficient *b*, found for compounds **5** and **6**, implies that HBA solvent effect exert through interactions of the 'lone' pair in OH groups on the outer phenyl with HBD probe in surrounding solvent shell. The negative value of *b* means bathochromic shift and greater stabilization of excited state with increasing HBA power of the solvent. Obtained results indicate that proton-donating capabilities of OH in *para*-position is significantly enhanced due to directional effect with pyridinium cation which causes increased proton-donating capability with respect to one in *meta*-position (-2.21 versus -1.41 , respectively). It should be noted that HBD probe exerts significantly weaker interactions with the nitro

Table 3 Results of the correlation analysis for compound **1–15** according to the Catalán equation

Comp.	$\nu_0 \times 10^{-3}$ (cm ⁻¹)	$c \times 10^{-3}$ (cm ⁻¹)	$d \times 10^{-3}$ (cm ⁻¹)	$b \times 10^{-3}$ (cm ⁻¹)	$a \times 10^{-3}$ (cm ⁻¹)	R^a	Sd^b	F^c	Solvent excluded from the correlation
1	25.77 ± 0.29	0.33 ± 0.33	0.92 ± 0.12	0.20 ± 0.12	0.72 ± 0.12	0.94	0.09	18.63	THF, EtAc, NMF, EtOH, DMA
2	27.13 ± 0.48	1.81 ± 0.61	1.80 ± 0.26	0.76 ± 0.21	-0.72 ± 0.19	0.96	0.13	22.98	DMA, AcN, dioxane, EtOH, NMP, THF
3	25.29 ± 0.23	0.04 ± 0.26	1.11 ± 0.13	0.41 ± 0.10	-0.50 ± 0.09	0.95	0.08	29.88	Dioxane, THF, EtAc
4	27.27 ± 0.27	-1.07 ± 0.33	0.87 ± 0.13	-0.22 ± 0.11	-0.48 ± 0.09	0.95	0.28	25.36	Dioxane, EtAc, AcN THF, EtOH
5	29.10 ± 0.71	-3.69 ± 0.87	0.67 ± 0.31	-2.92 ± 0.33	-1.63 ± 0.30	0.96	0.24	30.74	EtAc, iPrOH THF
6	27.73 ± 0.60	-0.37 ± 0.969	-0.81 ± 0.24	-1.50 ± 0.24	0.39 ± 0.24	0.93	0.17	14.93	NMF, DMA, DMSO, EtAc, THF
7	20.76 ± 0.29	-0.18 ± 0.32	1.20 ± 0.17	-0.29 ± 0.14	-0.13 ± 0.11	0.94	0.09	17.81	Dioxane, THF, EtAc, TCM
8	28.32 ± 0.24	-2.10 ± 0.28	-0.10 ± 0.10	-0.44 ± 0.10	-0.85 ± 0.10	0.96	0.07	30.89	DMSO, DMF, MeOH
9	30.44 ± 0.25	-0.97 ± 0.34	-0.23 ± 0.09	-0.41 ± 0.11	-0.55 ± 0.09	0.93	0.05	14.80	iPrOH, AcN, acetone, NMF, MeOH
10	33.11 ± 0.72	-2.31 ± 0.92	-0.57 ± 0.30	1.02 ± 0.32	-2.51 ± 0.36	0.93	0.22	16.20	NMF, acetone, MeOH, THF
11	19.17 ± 0.59	-1.98 ± 0.50	1.75 ± 0.43	-0.14 ± 0.20	-0.32 ± 0.21	0.95	0.14	35.20	Dioxane, DMA, THF, EtOH
12	28.91 ± 0.73	0.60 ± 0.73	-1.96 ± 0.45	-0.27 ± 0.38	1.76 ± 0.29	0.94	0.20	20.44	DMA, dioxane, iBuOH, EtAc, AcN
13	27.24 ± 0.29	-2.65 ± 0.36	-0.38 ± 0.10	0.27 ± 0.11	-0.70 ± 0.13	0.94	0.07	17.82	F, NMF, 1-BuOH, DMSO, iPrOH
14	22.83 ± 0.37	-1.26 ± 0.44	1.53 ± 0.20	0.25 ± 0.16	0.15 ± 0.15	0.95	0.12	26.90	Dioxane, EtAc, THF
15	24.29 ± 0.21	0.42 ± 0.26	0.53 ± 0.10	0.21 ± 0.09	0.43 ± 0.09	0.94	0.06	19.78	Dioxane, DMSO, MeOH

^aCorrelation coefficient^bStandard deviation^cFisher's test of significance

group of compound **12** with highest contribution of solvent dipolarity/polarizability.

Results of the quantitative separation of the non-specific solvent effect into polarizability and dipolarity term (coefficients c and d) performed using Catalán equation, Eq. (2), are given in Table 3. The results obtained by the use of Catalán equation provide better understanding of attractive/repulsive solvent/solute interactions and enable estimation of their appropriate contribution to ν_{\max} shift in UV-Vis spectra. Correlation results (Table 3) confirm that the solvent polarizability and dipolarity are the principal factors influencing the shift of ν_{\max} , whereas solvent acidity and basicity have moderate-to-low contribution. Synthesized compounds have permanent electric dipole moment due to symmetrical structure [17, 32], and, as it is expected, it is found that dipolar solvent-solute interactions have proper significance, i.e., compounds **2** (1.80), **11** (1.75), **12** (-1.96), and **14** (1.53). It can be assumed that superposition of the local dipole, i.e., polarized pyridinium cationic structure, and ones exerted by the substituent effect can contribute to larger dipolar solvent/solute interactions. It means that magnitude of dipolar interaction of the compounds increases with increasing electron-accepting potential of the substituent present in the outer rings, as well as with

the number of methoxy groups in the compounds **13–15**. The highest value of dipolar interaction for the compound **12** can be a consequence of superposition of two opposite electron-accepting effects of nitro group and pyridinium moiety. In general, dielectric properties of molecular framework under solvent influences can modify the π -electron density mobility which means that polarization effect is not necessarily transmitted in the direct line from the substituent to the probe sites.

The introduction of the substituents of different electronic properties (from electron accepting to electron donating) and the strength of their influence (strong, moderate, low.) causes appropriate enhancement/attenuation of π -electron mobility, and thus there is a wide range of the coefficient c values. The highest contribution of solvent polarizability is exerted for electron-rich substituents, which probably affect the mobility of π -electrons and more stabilize excited state relative to ground state. Proportional trend in the change of coefficient s and d is defined as follows: higher values of c correspond to lower values of d . Exceptions are noticed for compounds **2**, **4**, **11**, and **14**.

Specific solvent-solute interactions realized through hydrogen bonding are of less significance, except for the compounds **5**, **6**, and **10**, were high negative values of HBA

effect can be attributed to the OH groups. Both terms associated with the HBD and HBA influence of solvent (a and b) have different sign, and relatively low values/variation, while exceptions are found for compounds **5** and **10**.

Nature of molecular orbital: TD-DFT study

Mechanism of electronic excitations and changes in the overall charge distribution in both, ground and excited

states of the investigated molecules have been studied by calculation of the energies of frontier orbital ($E_{\text{HOMO}}/E_{\text{LUMO}}$) and energy gap (E_{gap}) values in gas phase, using B3LYP/Def2TZVP method. Obtained results are presented in Fig. 4 and Table S6. Compared to the unsubstituted molecule **1**, E_{gap} values generally decrease for the molecules with electron-donating substituents and increase for the compounds with electron-accepting substituents. Higher energy gap, observed for the strongest

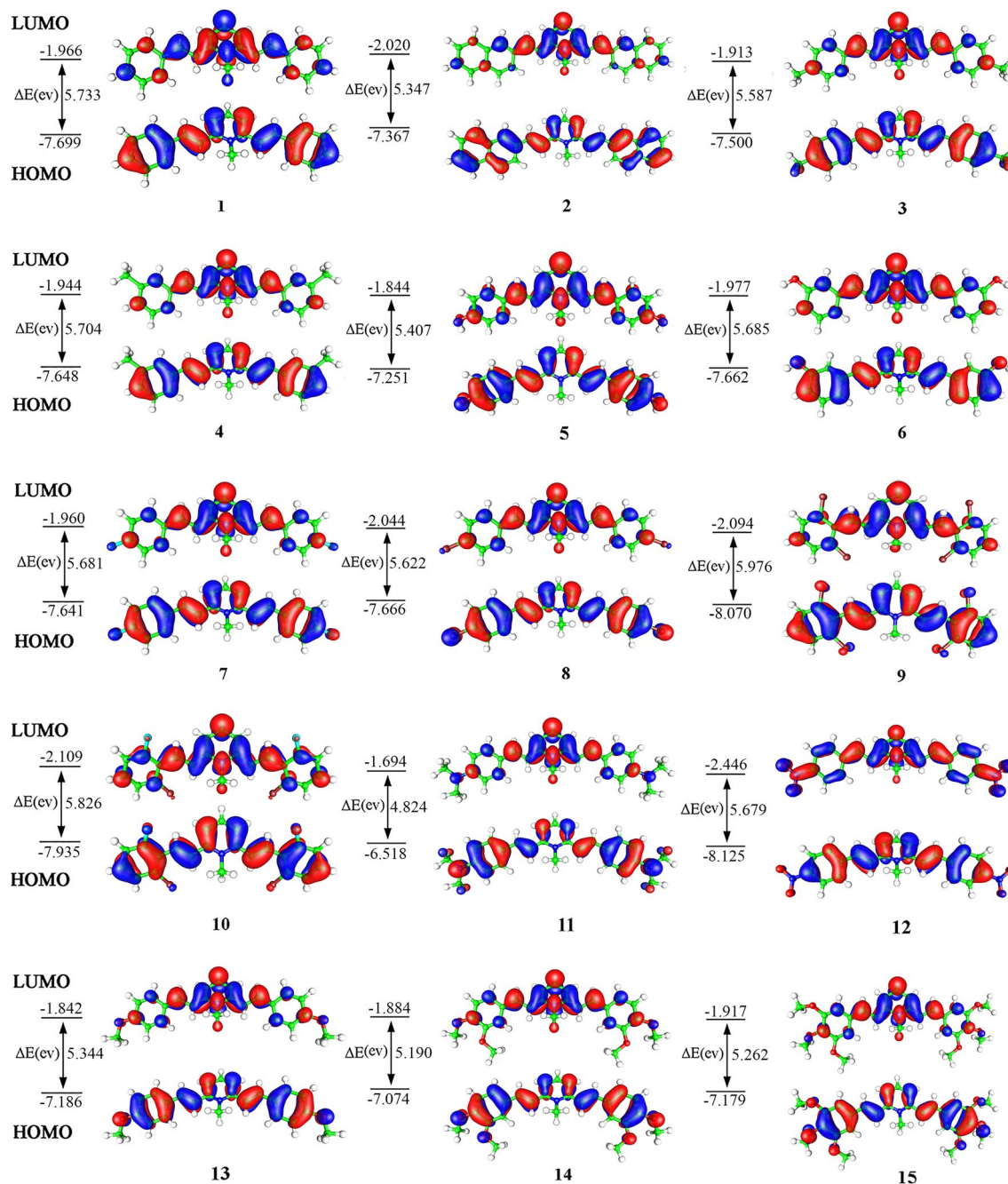


Fig. 4 The HOMO/LUMO orbitals and E_{gap} of compounds **1–15** in *s-trans/s-trans* form in DMSO

electron-acceptor substituted compound **12** and *ortho*-halogen disubstituted compounds **9** and **10**, is a consequence of higher HOMO orbitals stabilization, i.e., HOMO has lower energy compared to unsubstituted compound. Looking at the results of geometry optimization, given in Table S6, it is clear that these are compounds with the highest deviation from planarity.

As a consequence of N-methylation of the central pyridine ring, and the presence of the iodine counter ion, the *s-trans/s-trans* is the most stable conformation for all compounds. Qualitatively, HOMO of the parent compound and naphthyl substituted one is delocalized over the entire molecule, while LUMO is shifted towards the central pyridinium ring. The introduction of the weakly electron-donating methoxy groups in compounds **3** and **4** does not produce any appreciable change in the electron density of HOMO and LUMO orbitals with respect to compound **1**. The energy gap of these compounds is similar to the energy gap of compound **1**, although the involvement of the naphthyl moiety causes significant lowering of E_{gap} . On the other hand, the introduction of the strong electron-donating hydroxy group in compounds **5** and **6** causes a shift of the electron density of HOMO toward the outer phenyl rings. In addition, the introduction of the fluoro and chloro substituents, i.e., compounds **7–10**, and dimethylamino and nitro groups, i.e., compounds **11** and **12**, respectively, leads to similar electronic distribution in both HOMO and LUMO orbitals. Higher stabilization of both HOMO and LUMO orbitals cause that the energy gaps for the former compound are the highest, while lowest are found for compound **11**. In the compounds **13–15** both HOMO and LUMO orbitals are delocalized over its bent core in symmetrical fashion over methoxy substituted phenyl ring in former an over central pyridinium ring in later orbital. The results from theoretical calculation showed appropriate differences in optimized geometries of investigated compounds **13–15** regarding their conformational arrangement. The parallel orientation of *para*-OCH₃ in compound **13** with the plane of phenyl ring (dihedral angle 179.8°) provides condition for undisturbed interaction (moderate electron-donating character) of *p*-OCH₃ with π -electron density at neighboring phenyl ring. Oppositely, appropriate deviation (out-of-plane rotation) of this group in compound **14** (130.0°) causes decreased effective transmission of this interactions (attenuation effect) with undisturbed capability of methoxy group attached at C13 (179.9°). Significant steric repulsion (crowdedness) in compound **15** causes deviation of two OCH₃ groups attached at C11 and C12 carbons for 141.5° and 135.1°, respectively. Such preferred orientation influences decrease of electron-donating capability of *para*-OCH₃ group, and electron-accepting power of meta-OCH₃ attached at C11 (Scheme 1). Moreover, electronic substituent effect on electronic density can be seen in the overall charge distribution in HOMO/LUMO

orbitals (Fig. 4). Non-linear changes in the energy of HOMO and appropriate decrease of LUMO energy orbitals were observed. From the presented results it seems that complex contribution of substituent effects, interplay between present methoxy groups, position-dependent electronic effects and their spatial arrangement influences in a different way of HOMO/LUMO energies (E_{gap}) and energies of optimized structure (Table 1).

The ICT process is more feasible in compounds with increased π -electronic density, i.e., **2** and **13–15**. This is a consequence of higher polarizability, and thus the stability of excited state with respect to the ground state, under influences of surrounding solvent environment (Table 4). Due to this, the excited and ground states are closer and internal conversion takes place more effectively. Variation of structural/substituent patterns clearly indicates that contribution of both factors, structural and substituent/compound donor–acceptor characters, are involved in the ICT mechanism of the investigated molecules. Additional results from TD-DFT calculations in DMSO solution, oscillator strengths, vertical excitation energies and electronic transitions are provided in Table 4. TD-DFT results indicate a large contribution of single HOMO to LUMO excitations in ground state to first excited state transition (greater than 80% for all compounds; Table 4). It can, also, be noticed that, for all compounds, there is an appropriate participation of HOMO-1 to LUMO + 1 excitation (in the range 4.8–10.3%) and HOMO-2 \rightarrow LUMO (5.4, 4.4 and 2.3% for compounds **2**, **6**, and **14**, respectively) and HOMO-4 \rightarrow LUMO (in the range from 2.1 to 5.5% for compounds **3–9**, **11**, **13**, and **15**). In conclusion, for all compounds, most of the calculated E_{gap} values and TD-DFT results are in consistent with the experimental results from UV–Vis measurement.

Bond length and occupying coefficient for quantifying the push–pull effect in the studied compounds

The push–pull parameters, bond lengths $d/\text{Å}$ and occupation quotients π^*/π , of the partial C₇=C₈ (C₇=C_{8'}) double bond in the donor–acceptor linking chain C₂₍₆₎–C_{7(7')}=C_{8(8')}–C_{9(9')} are considered. Such analysis can envisage the geometrical arrangement of the studied compound. Larger twisting of the double bonds induces electron donation into the π^* orbital, which, on the other hand, means that lower values of occupation coefficients ($\pi^*_{\text{C}=\text{C}}/\pi_{\text{C}=\text{C}}$) indicate lower degree of deviation [34]. Calculated π^*/π quotients for compounds **1–15** and the values of C₇=C₈ double bond lengths (Table 5) indicate low twisting of symmetrical styryl moieties (Table S4). Correlation results of $d(\text{C}_7=\text{C}_8)$ versus π^*/π , given in Fig. 5 and Table 6, indicate that increasing donor–acceptor character of the compounds **1–15** cause increase in length of C₇=C₈ double bonds.

Table 4 Results of TD-DFT calculations for transitions from ground to first vertical excited state for *s-trans/s-trans* isomers in DMSO solution

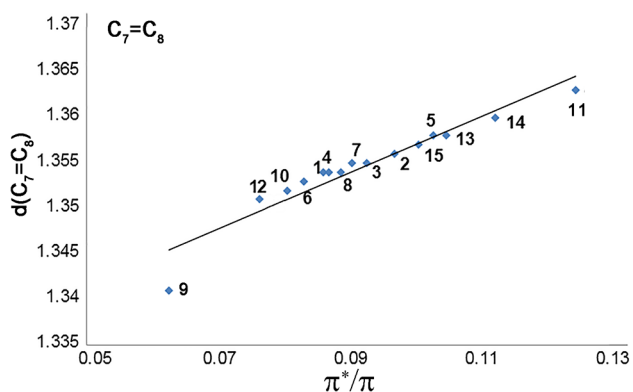
Comp. no.	Energy, (eV)	Oscillator strength	Excitation	CI expansion coefficient	% of single particle excitation contribution
1	3.3423	1.64	HOMO → LUMO	0.669	89.5
			HOMO-1 → LUMO+1	0.180	6.5
2	3.1425	2.33	HOMO → LUMO	0.633	80.1
			HOMO-1 → LUMO+1	-0.186	6.9
			HOMO-2 → LUMO	0.164	5.4
			HOMO-4 → LUMO	0.108	2.3
3	3.2372	1.81	HOMO → LUMO	0.665	88.4
			HOMO-1 → LUMO+1	0.189	7.1
			HOMO-4 → LUMO	-0.102	2.1
4	3.3243	1.68	HOMO → LUMO	0.667	90.0
			HOMO-1 → LUMO+1	0.177	6.3
5	3.1170	1.80	HOMO → LUMO	0.661	87.4
			HOMO-1 → LUMO+1	-0.196	7.7
			HOMO-4 → LUMO	0.114	2.6
6	3.3465	1.57	HOMO → LUMO	0.648	84.0
			HOMO-2 → LUMO	0.148	4.4
			HOMO-1 → LUMO+1	-0.155	4.8
			HOMO-3 → LUMO+1	-0.105	2.2
7	3.3134	1.66	HOMO → LUMO	0.667	90.0
			HOMO-1 → LUMO+1	-0.180	6.5
8	3.2810	1.87	HOMO → LUMO	0.662	87.6
			HOMO-1 → LUMO+1	-0.190	7.2
			HOMO-4 → LUMO	0.112	2.5
9	3.5346	1.46	HOMO → LUMO	0.663	87.9
			HOMO-1 → LUMO+1	0.167	5.6
10	3.4153	1.62	HOMO → LUMO	0.668	89.2
			HOMO-1 → LUMO+1	-0.183	6.7
11	2.7069	2.24	HOMO → LUMO	0.643	82.7
			HOMO-1 → LUMO+1	0.227	10.3
			HOMO-2 → LUMO	0.147	4.3
12	3.3543	1.97	HOMO → LUMO	0.646	83.5
			HOMO-1 → LUMO+1	-0.216	9.3
			HOMO → LUMO+2	0.133	3.5
13	3.0670	1.87	HOMO → LUMO	0.657	86.3
			HOMO-1 → LUMO+1	-0.202	8.2
			HOMO-4 → LUMO	0.102	2.1
14	2.9961	1.91	HOMO → LUMO	0.646	83.5
			HOMO-1 → LUMO+1	-0.209	8.7
			HOMO-2 → LUMO	0.108	2.3
			HOMO-4 → LUMO	-0.110	2.4
15	3.0685	1.90	HOMO → LUMO	0.645	83.2
			HOMO-1 → LUMO+1	-0.204	8.3
			HOMO-4 → LUMO	0.166	5.5

As can be seen in Fig. 5, compound **9** shows significant deviation from the correlation. The highest values of the dipole moment are obtained for the compounds with the, electron-acceptor, nitro substituents (Table 5). It is

known that molecules of higher hyperpolarizability have larger dipole moments, but the hyperpolarizability proves to be much higher for application as NLO molecules [35]. A possible approach to increase push-pull character is

Table 5 Occupation numbers of anti-bonding π^* and bonding π orbitals, bond lengths of the corresponding partial $C_7=C_8$ double bond, and dipole moments μ of compound **1–15**

Comp.	π	π^*	π^*/π	$d(\text{\AA})$ ($C_7=C_8$)	μ (Debye)
1	1.82526	0.15876	0.0870	1.350	0.8966
2	1.81746	0.17875	0.0984	1.353	1.5543
3	1.82137	0.17052	0.0936	1.352	0.8267
4	1.82415	0.16036	0.0879	1.351	1.1363
5	1.81816	0.18795	0.1034	1.354	1.8774
6	1.82614	0.15344	0.0840	1.350	1.4956
7	1.82530	0.16726	0.0916	1.351	2.7830
8	1.82407	0.16605	0.0910	1.351	3.4324
9	1.84253	0.12374	0.0672	1.345	0.9777
10	1.82999	0.15070	0.0824	1.350	1.1652
11	1.80429	0.22558	0.1250	1.360	1.2702
12	1.83057	0.14132	0.0772	1.348	7.3266
13	1.81621	0.19164	0.1055	1.355	1.5326
14	1.81328	0.20205	0.1114	1.356	2.2403
15	1.81553	0.19041	0.1049	1.355	4.4609

**Fig. 5** Correlation of bond lengths $d(C_7=C_8)$ in \AA and occupation coefficients π^*/π of the partial $C_7=C_8$ double bond in **1–15**

enhancement of the electron-accepting pyridinium group using strongly electron-donating substituents. A weaker double bond is assumed to be reflected by a longer distance between the donor and the acceptor groups. In that sense summary vector of the molecule arise, as a result of superposition of local vector (Fig. S5 represents overall contribution of local dipole moments assumed according electron-donating or accepting properties of substituents while Fig. S6 represents theoretically calculated summary vectors for molecules with the strongest donating and accepting substituents), while in case of compound **12** the same direction of all local vectors gave a summary vector with high value of dipole moments (Table 5).

Chemical shift differences, $\Delta\delta$, as a measure of the push–pull effect

The strong polarization of the double bond is also readily discernible by ^{13}C NMR due to extremely deshielded position of the alkenyl carbon on the donor side and the contrastingly shielded position of the carbon atom on the acceptor side of the push–pull alkene [34]. Chemical shift differences of the two sp^2 -hybridized carbons constituting the double bond ($\Delta\delta$) is an important property of push–pull molecules and it can be useful sensor of the corresponding push–pull effect. Higher values of $\Delta\delta_{C_7=C_8}$, as a measure of the push–pull effect, imply higher degree of resonance and the presence of electron donor substituents in the phenyl moiety.

Strongly activating electron donating groups (EDG) in the *p*-position of the phenyl substituted compounds **5** and **11** cause an increase in $\Delta\delta_{C_7=C_8}$. On the contrary, EDGs in the *m*-position of the phenyl ring (compound **6**) or presence of more than one EDG substituents, cause significantly lower increase relative to the unsubstituted compound **1**. Weakly activating EDGs as CH_3 in compounds **3** and **4** equally

Table 6 Results of correlations of selected bond distances versus π^*/π , $\Delta\delta_{C_7=C_8}$ and σ

Correlation	ρ	h	R	Sd	F	Comp. included in correlation	
$d(C_2-C_7)$ versus π^*/π	-0.274 ± 0.013	1.478 ± 0.001	0.986	0.0007	428.84	All	
$d(C_7=C_8)$ versus π^*/π	0.31 ± 0.03	1.33 ± 0.002	0.952	0.0015	127.31	All	
	0.24 ± 0.005	1.33 ± 0.0005	0.997	0.0002	2137	^a	
$d(C_8-C_9)$ versus π^*/π	-0.41 ± 0.045	1.49 ± 0.004	0.934	0.002	81.79	All	
$d(C_7=C_8)$ versus $\Delta\delta_{C_7=C_8}$	1.34 ± 0.002	0.0008 ± 0.0001	0.953	0.001	49.50	5, 6, 7, 8, 10, and 12	
	1.35 ± 0.0008	0.0005 ± 0.0007	0.973	0.0006	72.30	1, 3, 4, 11, 13, 14, and 15	
μ versus σ	$(2.42 \pm 0.32)\sigma^2$	$(3.76 \pm 0.18)\sigma$	2.80 ± 0.12	0.997	0.22	258.65	^b
	$(-2.97 \pm 0.07)\sigma^2$	$(2.26 \pm 0.05)\sigma$	1.28 ± 0.007	0.999	0.011	1241.68	^c

^aCompound **9** excluded^bCompound **15** excluded^cCompound **1** excluded

reduce $\Delta\delta_{C7=C8}$ value. In the case of halogen substituted compounds **7–10**, small influence of the electron donating group in the *o*-position, (compounds **9** and **10**) decrease π -electron delocalization and thus the $\Delta\delta_{C7=C8}$ value, relative to the *p*-substituted compounds **7** and **8**. Strong electron-accepting groups in compound **12** contribute to the lowest $\Delta\delta_{C7=C8}$ value.

Chemical shifts, given in Table S7, are correlated with the corresponding bond lengths, the third reliable push–pull effect indicator. Results are shown in the Supplementary Material (Fig. S7). With increasing push–pull character of the partial $C_7=C_8$ double bond, bond elongation, and increase in chemical shift differences $\Delta\delta_{C7=C8}$ are expected, and correlation still points into the right direction. The obtained correlation results are given in Table 6.

Linear free energy relationships (LFER) analysis of NMR data

The influence of the substituent effects on the electron density alteration over π -conjugative paths of ethylenic bonds is interested to study in line with push–pull character of investigated compounds. The linear free energy relationships (LFER) of NMR data provide better insight into the electronic effects on the electronic density shifts over studied molecule. LFER analysis has been used to postulate quantitative structure-properties relations of substituent effect on NMR data, and the best correlation results, obtained for C_2 , C_7 , C_8 , and C_9 carbons, are presented in Table 7 and Figs. S8–S11.

General conclusion derived from the results presented in Table 7 is that substituents on the benzene rings of investigated compounds influence chemical shifts of the carbon atoms of interest. The observed high values of proportionality constants, ρ , for these carbons indicate significant susceptibilities of the NMR chemical shifts to substituent electronic effects. Chemical shifts of C_7 and C_9 carbon atoms show normal effect with two separate correlations (Figs. S9 and S11), which means that deshielding of the observed carbon

increases with increase of electron-withdrawing strength of substituents.

This chemical shift alteration, i.e., alternation of ρ values (Table 7), is the consequence of the establishment of a strong interaction of donor–acceptor and acceptor–acceptor systems in which the pyridinium ring nitrogen acts as acceptor, and the introduction of a substituent of different properties cause an alternation of electron density at bridging structure (Figs. S5 and S6).

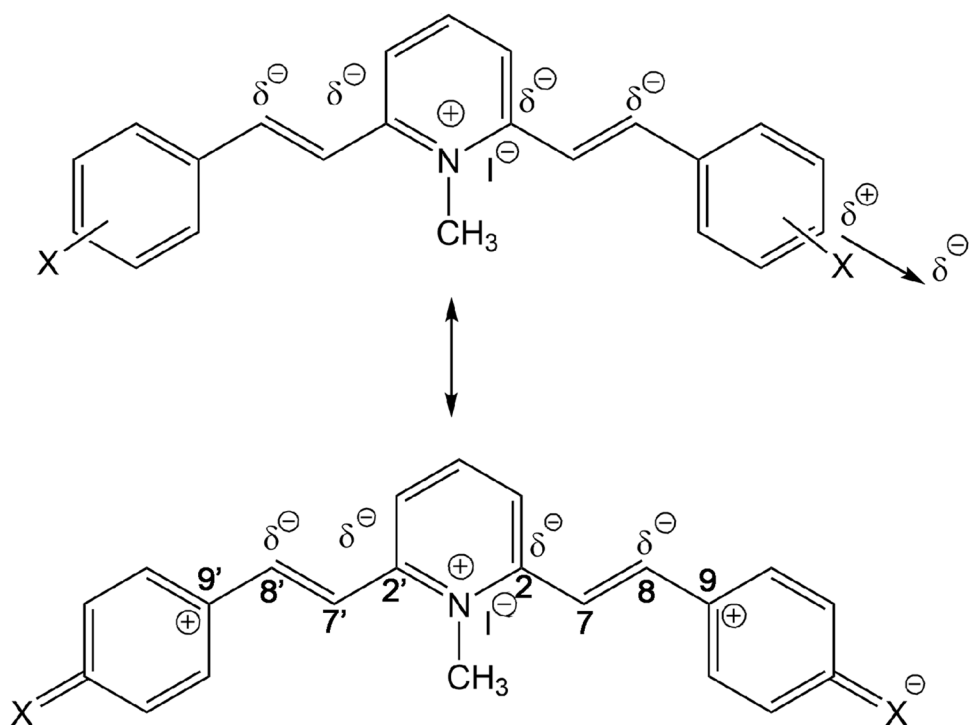
According to the NMR data *ortho*-substituted compounds **9** and **10**, shows the highest chemical shifts, in line with nitro-substituted compounds **12**. Steric effect includes all those phenomena which result in structural changes at measured sites, such as bond lengths and angles, effects due to size of the *ortho*-substituents. Due to that *ortho*-substituents exert larger influences on chemical shift, i.e., higher deshielding at all carbons considered, than electron donor and electron acceptor in 3- and 4-position. Spatial arrangement/deviation from planarity due to the presence of two halogen atoms in compounds **9** and **10** are in good accordance with the inter-atomic distances of those atoms taken from their optimized geometries. It is generally assumed that substituent effect at the *ortho*-position can be broadly classified as electronic, steric and anisotropic [36, 37] two former being the most significant.

High negative value of proportionality constants for C_2 (electron donor) and C_8 carbons indicates accumulation of positive charge on this atom with increasing electron donating capability of substituents. Explanation for the opposite effect of the substituents on C_2 and C_8 carbons (for electron donor) lies in the π -polarization concept introduced by Reynolds [38] and cross-polarization of methylated derivatives,[18] explained by appropriate resonance structures with contribution of π -polarization. The field effect, induced by substituent dipole, causes secondary π -electrons polarization in the subsequent independent π -electronic system without net π -electron transfer (Fig. 6). This concept of localized π -polarization and extended polarization is used for explanation of polar substituent effects within aromatic side-chain derivatives.

Table 7 Correlation results of the NMR data of studied compounds with σ constants obtained using Hammett Eq. (3)

Atom	ρ	h	R	F	Sd	Comp. excluded from correlation
C_2	-3.15 ± 0.41	153.22 ± 0.21	0.975	58.05	0.29	5, 6
	4.79 ± 0.61	153.22 ± 0.31	0.976	61.20	0.48	3, 10
C_7	3.01 ± 0.38	126.50 ± 0.20	0.970	63.86	0.45	–
	2.63 ± 0.45	124.05 ± 2.63	0.932	33.25	0.41	12
C_8	-5.38 ± 0.41	140.50 ± 0.18	0.978	172.90	0.59	1, 3, 4, 12
C_9	4.36 ± 0.50	141.93 ± 0.23	0.962	73.88	0.65	5
	3.07 ± 0.72	134.82 ± 3.07	0.925	17.85	0.85	–

Fig. 6 Resonance structures of electron-acceptor substituted compounds with contribution of π -polarization



In structure (1) (Fig. 6), presence of an electron-acceptor substituent induce a dipole on C–X. Electron-accepting effect of induced dipole transmitted through the molecular structure causes polarization of individual π units (localized polarization) [Fig. 6; structure (2)]. The experimental results can also be rationalized with the aid of the resonance polarization concept of the entire conjugated system (extended polarization). Resonance interaction in extended conjugated system of studied compounds has an opposite effect to the polarization caused by electron-acceptor substituent. The net result is that the electron-acceptor substituents increase the electron density on C₂ (C_{2'}) and C₈ (C_{8'}) carbons, hence, an increase in the shielding. Reverse substituent effect is operative at C₂ for electron donor and C₈ for all substituents. *ortho*-Substituents of high electron-accepting power cause a higher deshielding due to both, electron-withdrawing and *ortho*-effect.

The presentation of π -electronic conjugation throughout such molecules, as help in understanding specifics behavior of the change of chemical shifts of observed carbons, is given by resonance structures in Fig. S12 (Supplementary Material). Due to their particular position in the molecule, on the C₂ carbon atom reverse effects have influence. First, pyridine nitrogen, due to vicinity, tends to decrease electron density with its accepting properties (structure **d**) while, on the other hand, π -resonance effect of the styrene part of the molecule tends to increase electron density (structures **e–h**). In addition, positive charge also occurs on the C8 carbon

(structure **e**), at which reverse substituent effect is obtained (Table 4).

From the values of dihedral angles in Table S4, appropriate deviation from the planarity indicates that transmission of the resonance effect from substituted phenyl ring can be suppressed to some extent. Resonance interaction in extended resonance system can, thus, be achieved by π , π -conjugation, depending on the present substituent. In general, electron-acceptor attracts electron density from pyridinium ring causing an electron density shift over ethylenic bond. Opposite is true for the electron-donor-substituted compounds. Electron-donor substituents support electron-accepting resonance interaction in the pyridinium unit thus deshielding effect at C₂ is a result of a type of a “push-effect” of electron-rich phenyl ring, reflected through increased electron density at C₇ and C₉ carbons.

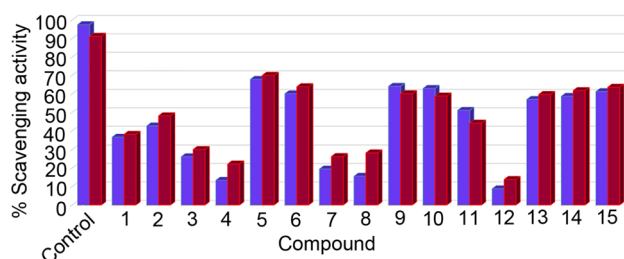


Fig. 7 Scavenging activity of investigated compounds **1–15** obtained DPPH (filled blue square) and ABTS (filled red square)

Antioxidant activity

The studied compounds shows wide variation of antiradical activity by inhibiting DPPH radical. The interaction of synthesized compounds with the stable DPPH free radical indicates their free radical scavenging ability, i.e., antiradical activity of compounds (Fig. 7). The majority of compounds show good antioxidant properties, and the maximum antioxidant activity is observed for compounds in the following order **5** > **9** > **10** > **6** > **15** > **14** > **13** > **11**. These compounds display more than 50% inhibition, which is comparable to that of the standard (vitamin C) at a similar concentration. It is assumed that higher capacity/ability of compounds to lose hydrogen, i.e., creation of structurally stable radical is correlated with higher scavenging activity of the studied molecule. In addition, it is expected that structure of the compounds and electronic properties of substituents have a crucial role to the stabilization of generated radical [39, 40]. The presence of either electron-withdrawing or electron-donating groups in the aromatic rings and the presence of a pyridine ring may play a functional role in the activity [41, 42]. It is also demonstrated that antioxidant activity is related to the number of induced substituent groups [5]. Therefore, the difference in the activity of the synthesized compounds is not unexpected.

The eight moderate active compounds possess some special structural features that can be depicted in the following, explaining the relationship between structure and activity. Both distyryl derivatives with hydroxyl group in the *meta*- or *para*-positions on the phenyl ring, i.e., compounds **5** and **6**, respectively, show good activity (60.03 and 67.77%, respectively). However, *meta* hydroxy substituted compound (**6**) shows lower activity. Addition of methoxy group at *para* position (**13**) significantly improves antioxidant activity. This result can be explained by the strong electron donation ability of the hydroxyl group in *para* positions while this group in *meta*-position shows negligible electron-accepting character [43]. The results are confirmed by the successive addition of another methoxy group in *meta*-position (compounds **14** and **15**). Hypothetically, the electron donating group should increase the electronic density in the styryl part of the molecules. It is well established that this type of groups stabilize the resulted styryl radicals through the resonance effect (as in methoxy substituted derivatives **13–15**), thus lower the C-H bond energy in styryl part of the molecules and enhance the radical scavenging activity [43]. On the basis of the results it can be concluded that apart from the position of the electron donating group in the phenyl ring, the activity of the compound is influenced by the number of groups, i.e., increased number of methoxy groups in phenyl rings contributes to increase in antioxidant activity.

Contrarily, the presence of an electron-withdrawing group might destabilize the styryl moiety by withdrawing electronic

density and may lead to decrease in the antioxidant potential. This phenomenon is observed for compounds **7**, **8**, and **12**, were F, Cl and NO₂ electron-withdrawing groups, respectively, lower the antioxidant potential. In contrast to *para* halogen monosubstituted phenyl rings in styryl derivatives, the presence of two halogen element in the *ortho*-position of the phenyl ring strongly increases antioxidant activity (**9** and **10**). In addition, antioxidant activity of all compounds is measured using ABTS assay, and the results are presented in Fig. 7 The tested compounds shows similar trend in antioxidant activity as with DPPH method.

Conclusions

This work reports synthesis, spectral, and antioxidant properties of 15 symmetrical heterocyclic derivatives of 1-methyl-2,6-bis[2-(substituted phenyl)ethenyl]pyridinium iodides. The presence of double bond between two aromatic moieties connected to central pyridinium ring provides means for rotation and existence of synthesized compounds in different conformers. Theoretical calculations show that *s-trans/s-trans* form is dominant isomer for all synthesized derivatives.

Understanding the transmission of substituent electronic effect by π -polarization mechanism is one of the goals of the present investigation. Solvatochromic properties are analyzed from the UV–Vis absorption spectra recorded in the solvents of different polarity. LSER correlation results indicate that increasing solvent polarity induce red shift of the absorption spectra. Solvatochromic behavior of compounds **1–15** can be, in a considerable extent, ascribed to the non-specific electrostatic interactions with the solvent, rather than to the specific hydrogen bonding. Such behavior most probably stems from the high symmetry of the investigated compounds. The influence of substitution, hydrogen bonding, and protonation states on spectral and photophysical properties are described, along with the analysis of the frontier orbitals of studied molecules, obtained from calculations performed on TD-DFT level of theory. Bond length of C₇=C₈ (C₇=C₈), occupation quotients π^*/π of that bond and $\Delta\delta_{C7=C8}$ are found to be applicable sensors of the donor–acceptor character of the studied molecules.

As for the antioxidant properties all compound possess moderate scavenging effect. The results of the antioxidant screening by ABTS radical scavenging assay have revealed better antioxidant activity compared to DPPH activity assay.

Acknowledgements The authors acknowledge financial support from the Ministry of Education, Science and Technological development of Serbia, Project no. OI 172013.

Compliance with ethical standards

Conflict of interest The authors declare that they have no conflict of interest.

References

- V.G. Pivovarenko, A.V. Grygorovych, V.F. Valuk, A.O. Doroshenko, *J. Fluoresc.* **13**, 479 (2003)
- C.G. Fortuna, V. Barresi, C. Bonaccorso, G. Consiglio, S. Failla, A. Trovato-Salinario, G. Musumarra, *Eur. J. Med. Chem.* **47**, 221 (2012)
- M. Fichera, L. Gregoli, G. Musumarra, *J. Phys. Org. Chem.* **13**, 344 (2000)
- V. Barresi, D.F. Condorelli, C.G. Fortuna, G. Musumarra, S. Scirè, *Bioorgan. Med. Chem.* **10**, 2899 (2002)
- E. Bendary, R.R. Francis, H.M.G. Ali, M.I. Sarwat, S. El, Hady, *Ann. Agric. Sci.* **58**, 173 (2013)
- M. Mojarrab, R. Soltani, A. Aliabadi, *J. Nat. Pharm. Prod.* **8**, 125 (2013)
- F. Azarbani, A. Kakanejadifard, V. Nadri, S. Kakanejadifard, *J. Iran. Chem. Soc.* **14**, 201 (2017)
- B. Carlotti, E. Benassi, A. Spalletti, C.G. Fortuna, F. Elisei, V. Barone, *Phys. Chem. Chem. Phys.* **16**, 13984 (2014)
- B. Carlotti, I. Škorić, M. Šindler-Kulyk, U. Mazzucato, A. Spalletti, *J. Photochem. Photobiol. A Chem.* **244**, 38 (2012)
- G. Soriano-Moro, M.J. Percino, A.L. Sánchez, V.M. Chapela, M. Cerón, M.E. Castro, *Molecules* **20**, 5793 (2015)
- M.R.S.A. Janjua, *J. Iran. Chem. Soc.* **14**, 2041 (2017)
- A.I. Vokin, A.M. Shulunova, T.N. Aksamentova, G.V. Bozhenkov, V.K. Turchaninov, *Russ. J. Gen. Chem.* **76**, 596 (2006)
- J.M. Marković, N.P. Trišović, D. Mutavdžić, K. Radotić, I.O. Juranić, B.J. Drakulić, A.D. Marinković, *Spectrochim. Acta Part A Mol. Biomol. Spectrosc.* **135**, 435 (2015)
- S. Feng, Y. Kyung Kim, S. Yang, Y.-T. Chang, *Chem. Commun.* **46**, 436 (2010)
- I. Baraldi, E. Benassi, S. Ciorba, M. Šindler-Kulyk, I. Škorić, A. Spalletti, *Chem. Phys.* **361**, 61 (2009)
- L. Giglio, U. Mazzucato, *Phys. Chem. Chem. Phys.* **2**, 4005 (2000)
- A. Spalletti, *Spectrochim. Acta Part A* **59**, 75 (2003)
- H. Wang, R. Helgeson, B. Ma, F. Wudl, *J. Org. Chem.* **65**, 5862 (2000)
- N.R. Penthala, J. Eldridge, T.R.Y. Reddy, S. Parkin, P.A. Crooks, *Acta Crystallogr. Sect. E Struct. Rep. Online* **66**, o1793 (2010)
- X. Xu, W. Qiu, Q. Zhou, J. Tang, F. Yang, Z. Sun, *J. Phys. Chem. B* **112**, 4913 (2008)
- F. Weigend, R. Ahlrichs, *Phys. Chem. Chem. Phys.* **7**, 3297 (2005)
- T. Yanai, D.P. Tew, N.C. Handy, *Chem. Phys. Lett.* **393**, 51 (2004)
- J. Tomasi, *Theor. Chem. Acc.* **112**, 184 (2004)
- F. Weinhold, J.E. Carpenter, in *The structure of small molecules and ions* ed. by R. Naaman, Z. Vager (Springer, Boston, MA, 1988), pp. 227–236
- M.J. Frisch, G.W. Trucks, H.B. Schlegel, G.E. Scuseria, M.A. Robb, J.R. Cheeseman, G. Scalmani, V. Barone, B. Mennucci, G.A. Petersson, H. Nakatsuji, M. Caricato, X. Li, H.P. Hratchian, A.F. Izmaylov, J. Bloino, G. Zheng, J.L. Sonnenberg, M. Hada, M. Ehara, K. Toyota, R. Fukuda, J. Hasegawa, M. Ishida, T. Nakajima, Y. Honda, O. Kitao, H. Nakai, T. Vreven, J.A. Montgomery Jr., J.E. Peralta, F. Ogliaro, M. Bearpark, J.J. Heyd, E. Brothers, K.N. Kudin, V.N. Staroverov, R. Kobayashi, J. Normand, K. Raghavachari, A. Rendell, J.C. Burant, S.S. Iyengar, J. Tomasi, M. Cossi, N. Rega, J.M. Millam, M. Klene, J.E. Knox, J.B. Cross, V. Bakken, C. Adamo, J. Jaramillo, R. Gomperts, R.E. Stratmann, O. Yazyev, A.J. Austin, R. Cammi, C. Pomelli, J.W. Ochterski, R.L. Martin, K. Morokuma, V.G. Zakrzewski, G.A. Voth, P. Salvador, J.J. Dannenberg, S. Dapprich, A.D. Daniels, Ö. Farkas, J.B. Foresman, J.V. Ortiz, J. Cioslowski, D.J. Fox, Gaussian 09 (Gaussian Inc, Wallingford CT, 2009)
- Y. Marcus, *Chem. Soc. Rev.* **22**, 409 (1993)
- J. Catalán, *J. Phys. Chem. B* **113**, 5951 (2009)
- C. Hansch, A. Leo, R.W. Taft, *Chem. Rev.* **91**, 165 (1991)
- G. Bartocci et al., in *Conformational analysis of molecules in excited states*, ed. by J. Waluk (Wiley, New York, 2000), pp. 237–296
- V.M. Chapela, M.J. Percino, C. Rodríguez-Barbarín, *J. Chem. Crystallogr.* **33**, 77 (2003)
- M. Mirzaei, *Zeitschrift Fur Naturforsch. Sect. A J. Phys. Sci.* **65**, 844 (2010)
- I. Baraldi, G. Ginocchietti, U. Mazzucato, A. Spalletti, *Chem. Phys.* **337**, 168 (2007)
- L. Wang, Y. Feng, J. Xue, Y. Li, *J. Serbian Chem. Soc.* **73**, 1 (2008)
- E. Kleinpeter, S. Klod, W. Rudorf, *J. Org. Chem.* **69**, 4317 (2004)
- E. Kleinpeter, B.A. Stamboliyska, *Tetrahedron* **65**, 9211 (2009)
- V. Nummert, M. Piirsalu, V. Mäemets, S. Vahur, I.A. Koppel, *J. Phys. Org. Chem.* **22**, 1155 (2009)
- J. Oszczapowicz, *Int. J. Mol. Sci.* **6**, 11 (2005)
- W.F. Reynolds, A. Gomes, A. Maron, D.W. MacIntyre, A. Tanin, G.K. Hamer, I.R. Peat, *Can. J. Chem.* **61**, 2376 (1983)
- R. Apak, M. Özyürek, K. Güçlü, E. Çapanoğlu, *J. Agric. Food Chem.* **64**, 1028 (2016)
- K. Battula, S. Narsimha, V. Nagavelli, R. Srinivasa, *J. Serbian Chem. Soc.* **81**, 88 (2016)
- M.A. Al-Omar, A.R. Sayed, M.M. Youssef, *Molecules* **20**, 2591 (2015)
- A. Božić, N. Filipović, I. Novaković, S. Bjelogrić, J. Nikolić, S. Drmanić, A. Marinković, *J. Serbian Chem. Soc.* **82**, 495 (2017)
- M.A. Saleh, A.M. El-Gizawy, R.E.L. El-Bassiouny, H.M. Ali, *Ann. Agric. Sci.* **58**, 239 (2013)